4-1-2009

Poly[4(5)-vinylimidazole]/polyvinylidene fluoride composites as proton exchange membranes

Jingjing Pan

Poly[4(5)-Vinylimidazole]/Polyvinylidene Fluoride Composites as Proton Exchange Membranes

Jingjing Pan

April 2009

Thesis submitted in partial fulfillment of the requirements for the degree of Master of Science in Chemistry.

Approved: _____

Thomas W. Smith (Advisor)

_____

Paul Rosenberg (Department Head)

Department of Chemistry
Rochester Institute of Technology
Rochester, New York 14623-5603

Copyright Release Form:

INVESTIGATION OF POLY[4(5)-VINYLIMIDAZOLE] COMPOSITES AND THEIR POTENTIAL AS PROTON CONDUCTIVE MEMBRANES

Jingjing Pan

April, 2009

Abstract

In the present research, the morphology and thermal chemical characteristics of composite films comprised of poly(vinylidene fluoride) (PVF_2) and poly[4(5)-vinylimidazole/vinylimidazolium trifluoromethylsulfonylimide] (PVIm/VIm^+TFSI^-]) were studied. In these composites, conditions such as choice of solvent and drying and annealing conditions can affect the crystal habit, crystallite size and degree of crystallinity of PVF_2 as well as the distribution of the minor component, poly[4(5)-VIm/VIm^+TFSI^-]. Such composites may have potential in fuel cells as high-temperature proton-exchange membranes.

When cast from either dimethylformamide (DMF) or dimethylacetamide (DMAC) at ambient temperature and dried at temperatures below 100˚C, PVF_2 homopolymer films and PVF_2//PVIm/VIm^+TFSI^- composite films were obtained in which the crystallites of PVF_2 were β-phase. The films initially obtained were white, opaque films with limited strength and mechanical integrity. After heating to 200˚C, both the PVF_2 films and the PVF_2//PVIm/VIm^+TFSI^- films became stronger and more transparent. X-ray diffraction showed that prior to heating the PVF_2 homopolymer film was β-phase and after heating to 200˚C PVF_2 was α-phase. This was also the case with the PVF_2//PVIm/VIm^+TFSI^- composites. In other words, the crystalline polymorph of PVF_2 in the non-heated composite films was identical to that of non-heated homopolymer PVF_2, and the PVF_2 polymorph in the heated composite films was identical to that of heated homopolymer PVF_2 films. DSC analysis showed that the melting point of crystals in heated PVF_2 was lower than that in the non-heated PVF_2. This difference in T_m (melting temperature) is attributed to the fact that PVF_2 β-phase crystals have a higher melting temperature than that of the α-phase crystals. PVF_2 composites cast from DMAC have a higher onset T_c (onset crystallization temperature) than do PVF_2 composites cast from DMF. The crystallinity of PVF_2 in the heated homopolymer films was lower than that in the non-heated films. The percent crystallinity in the composites was variable and depended, to some degree on the level of TFSI. In the composites cast from DMAC, the crystallinity is maximal at 15 mol% TFSI and decreases somewhat as the TFSI level is increased to 50 mol%. The crystallinity of PVF_2 in the composites cast from DMF is minimal at 15 mol % TFSI and increases in concert with the TFSI level. The intimacy of the phases in the composites was assessed by evaluating the amount of PVIm/VIm^+TFSI^- that could be extracted with ethanol/water. It was found that, after heating, the amount of imidazole polymer that could be extracted dropped from about 81% to less that 16% of the imidazole polymer originally in the mixture. This observation coupled with the substantial transparency of the heated composites, is indicative of a nanoscopic composite in which the PVIm/VIm^+TFSI^- phase is intimately mixed with the amorphous phase of the majority PVF_2 component.

Table of Contents

Acknowledgements

First of all, I would like to thank Dr. Thomas W. Smith, my advisor, for helping me to learn about polymers and for his patience. The support of Dr. Paul Rosenberg, Head of the Department of Chemistry, and Ms. Brenda Mastrangelo, Academic Advisor in the Department of Chemistry, for their support during my graduate career has been particularly appreciated. I would like to thank Dr. Andreas Langner, Dr. Christopher Collison and Dr. Massoud Miri for being my thesis committee members and for their advice. I also would like to thank my fellow graduate students whom I have worked beside during the past three years. I am grateful to Dr. Surendra K Gupta for his assistance with X-ray diffraction and I thank Mr. Tom Alston for his help with DSC measurements.

As for National Technology Institute of Deaf (NTID), I greatly thank the National Technical Institute of Technology (NTID) Professionals and especially Dr. Dianna Brook for providing me with an academic fellowship during my graduate career. I want to give many thanks to Chairperson at the Department of Science & Mathematics, Dr. Vince Daniele, for his support and understanding. I'm so thankful to Ms. Gail Binder, my retired chemistry professor and advisor who made me love chemistry deeply and has been encouraging during my graduate school years. Also, I am grateful that Dr. Matthew Lynn, my current advisor, he has been supporting me and encouraging since Ms. Binder was retired. I want to take this opportunity to thank my sign language interpreter Cheryl Reminder for her work to help me in communication. Lastly, I must remember Ms. Sharon Rasmussen who was chairperson of NTID the Department of Science & Mathematics Support and tragically passed away last year.

I want to express by gratitude to Professor Dr. Peggy Cebe from Tuft University, my first mentor who inspired me and led me into the world of polymers for the first time.

My family is far away from me and I have not seen them for many years. I thank my parents, Yulin and Junying, and my brother Fanping for their love and encouragement.

All in all, I have had many wonderful memories at RIT. I will remember wonderful people here and cherish the memories in my life.

List of Tables

List of Figures

List of Abbreviations

BPO - Dibenzoyl peroxide

DMF - N,N'-dimethylformamide

TFSI - Trifluoromethanesulfonylimide

DMAC - Dimethylacetamide

AIBN - Azobisisobutyronitrile

PVF_2 - Poly(vinylidene fluoride)

PVIm - Poly[4(5)-vinylimidazole]

$PVIm^+$ - Poly[4(5)-vinylimidazole/imidazolium]

DSC - Differential Scanning Calorimetry

PVF_2//PVIm/Im^+TFSI^- - Poly(vinylidene fluoride)//poly[4(5)-vinylimidazole/imidazolium-trifluoromethanesulfonylimide]

I. Introduction and Background

Global warming is a serious environmental problem due, in large part, to increases in emissions of air pollutants and greenhouse gases.[1] Mankind is also faced with a limited supply of fossil fuels and as global consumption increases environmental and economic problems are projected to become much worse.[2] One way to solve this problem is through the use of alternative fuels. Hydrocarbon-powered combustion engines can be replaced by proton exchange membrane fuel cells, which use hydrogen as a fuel and emit only water. Since hydrogen can be obtained by electrolysis of water, fuel cells can be a clean energy alternative to the above problems.

A. **The proton exchange membrane fuel cell**

A fuel cell is an electrochemical device that converts chemical energy stored in hydrogen or gasoline into electricity. In 1839, the Welsh scientist Sir William Robert Grove[3] developed the first fuel cell, the "gas voltaic battery", which combined hydrogen and oxygen and produced electric energy. He is known as the "Father of the Fuel Cell". A proton-exchange fuel cell consists of two catalytic electrodes (an anode and a cathode), separated by a hydrogen ion selective electrolyte, and connected by a wire to complete the electrical circuit. An illustration of a typical fuel cell is shown in Figure 1.

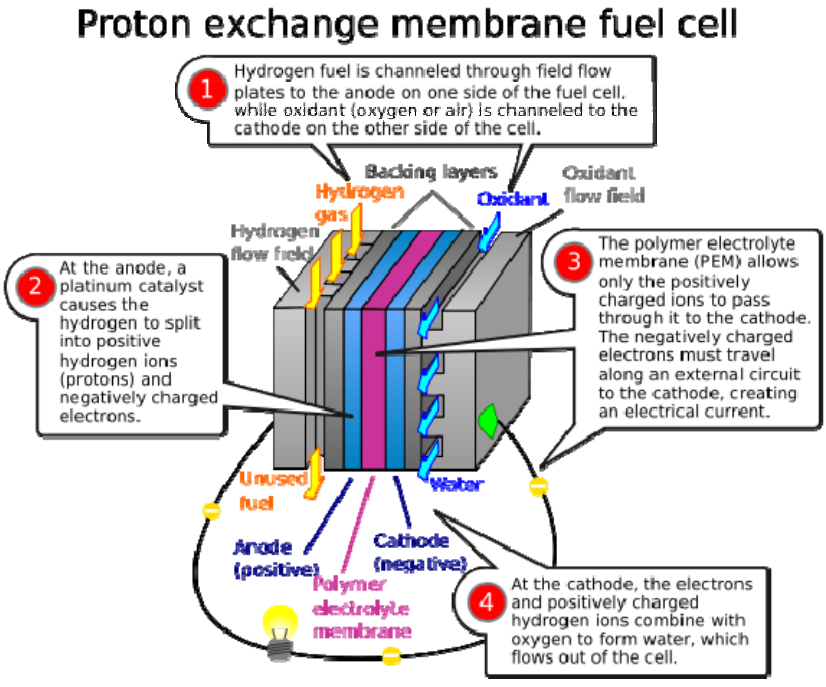

Figure 1. Illustration of a PEM fuel cell[4]

At the anode, hydrogen is oxidized to produce protons and electrons. The oxidation reaction is promoted by a platinum catalyst embedded in the anode.

Oxidation at anode: $H_2 \rightarrow 2H^+ + 2e^-$

The H^+ ions pass through the electrolyte membrane to the cathode where oxygen is reduced and combined with H^+ to produce water.

Reduction at cathode: $\frac{1}{2} O_2 + 2H^+ + 2e^- \rightarrow H_2O$

Protons permeate through the ion selective membrane and electrons produced at the anode are transported via an external circuit.

Overall cell reaction: $H_2 + 1/2O_2 \rightarrow H_2O$

Common types of fuel cells include polymer electrolyte membrane fuel cells (PEMFC), direct methanol fuel cells (DMFC), alkali fuel cells (AFC), phosphoric acid fuel cell (PAFC), solid oxide fuel cells (SOFC) and molten carbonate fuel cells (MCFC).[5] The PEMFC uses a solid polymer membrane as an electrolyte and uses platinum as a catalyst. It usually operates at low temperature (60-100˚C). Hydrogen gas is the main source of hydrogen fuel. Platinum catalysts are expensive and poisoned easily by CO from hydrocarbon fuels. The DMFC uses liquid methanol fuel instead of hydrogen. It operates at slightly higher temperature (50-120˚C). Small mobile power applications such as laptops and cell phones use DMFC, but current limitations such as membrane corrosion and fuel crossover must be addressed. The PAFC uses liquid phosphoric acid as an electrolyte with a platinum catalyst. It usually operates at high temperature (150-200˚C) and is tolerant to impurities. Typically it is used for medium to large scale stationary power generation. The AFC uses hydrogen gas as a fuel. It operates in an electrolyte solution of potassium hydroxide. The operating temperature is 23-250˚C with a variety of metal catalysts. But the AFCs are subject to CO poisoning. The SOFC uses a solid ceramic electrolyte and operates at 800-1000˚C. It is tolerant to CO poisoning. The MCFC uses a molten alkali carbonate mixture for an electrolyte and can operate at 600-750˚C. Both SOFC and MCFC have limitations including slow start up and the requirement of durable materials for high temperature[6].

A proton exchange membrane (PEM) is semipermeable, allowing protons to pass through while being impermeable to molecules of oxygen and hydrogen gas. PEMs may be single

component or composite (multi-component) polymer membranes in which one component is a strong acid ionomer. The PEM is used to separate the two catalytic reactions, oxidation of hydrogen at the anode and reduction of oxygen at the cathode while simultaneously allowing protons to pass through as electricity is generated.

The benchmark materials for PEMs are perfluorinated ionomer membranes typified by DuPont's Nafion®. This compound was discovered in the late 1960's by Walther Grot at Dupont[7] and is one of the most common and commercially available materials for PEM. Nafion® is a sulfonated tetrafluorethylene copolymer and has a perfluoroethylene backbone with a sulfonated perfluoroether side chains. A representative structure for Nafion® is shown in Figure 2.

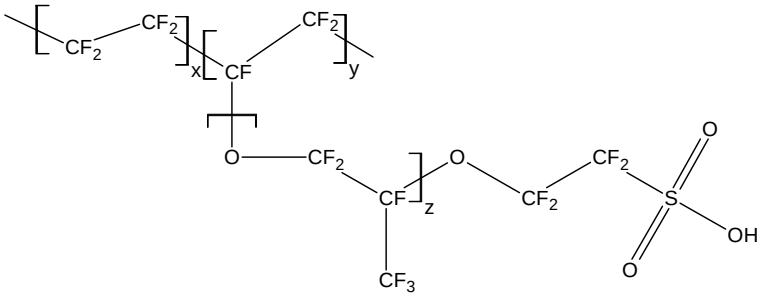

Figure 2. Structure of Nafion

The tetrafluoroethylene backbone provides excellent thermal, mechanical, and chemical/oxidative stability while the sulfonic acid group provides the functionality for proton conductivity. Because of its superior ion mobility and chemical and thermal stability, Nafion® has found widespread application in fuel cells and in chlor-alkali production. It is reported that the proton conductivity of these perfluorosulfonic acid polymer membranes with thicknesses of 25 to 175 μm at 80°C and 100% relative humidity (RH) is on the order of 10^{-1} Scm^{-1}.[8]

Kreuer studied the microstructure of perfluorosulfonic polymers and noticed some rather interesting properties that these materials possess. He reported that proton conductivity strongly increases when the concentration of absorbed water increases. The transport of protons and water is related to the microstructure and water content of the Nafion® membrane. When Nafion® is hydrated, the sulfonic acid functional groups ionize and aggregate to form hydrophilic domains

through which protons and water can be transported. The hydrophobic backbone provides for chemical and thermal stability, and being insoluble in water maintains the structure and integrity of the membrane. Figure 3 depicts architectural components of the Nafion® membrane.

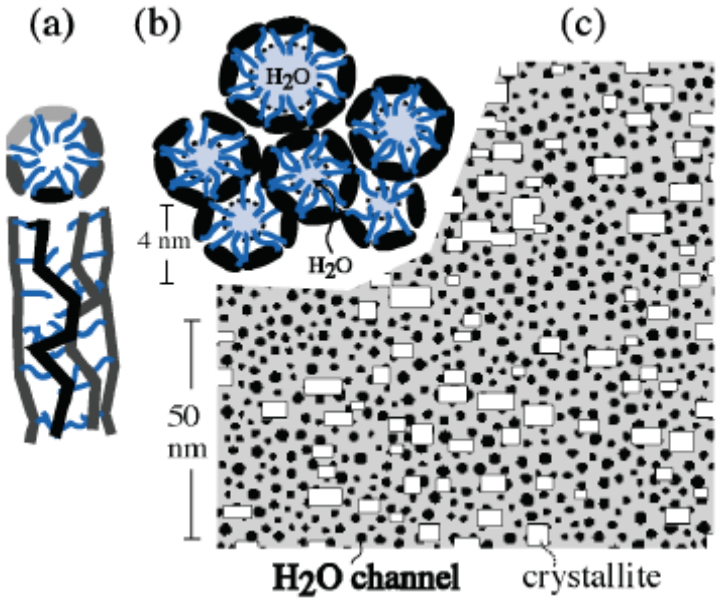

Figure 3. Architectural Elements of Nafion®[9]

Because of their excellent proton conductivity and mechanical strength, sulfonic acid membranes of varying kind have been extensively studied as PEMs. Sulfonated aromatic polymers that have been employed include poly(etheretherketone) (PEEK) and poly(ether ketone) (PEK). Figure 4 shows the relative conductivity of a variety of materials in which the temperature dependence of proton conductivity has been studied. One can see that sulfonated polymers like Nafion®, exhibit high proton conductivity, above 10^{-1} Scm^{-1}, at temperature below 100˚C. The benzimidazole/H_3PO_4 liquid membrane exhibits high proton conductivity at high temperature but below the level of $1x10^{-1}$ Scm^{-1} provided by the hydrated sulfonic aid polymers.

Figure 4 also shows the temperature dependence of proton conductivity in a variety of ethoxylated imidazole oligomers and a composite of sulfonated PEEKK + imidazole that Kreuer et al have explored because of their potential as models for membranes that might function at a temperature in excess of 100˚C and low relative humidity.

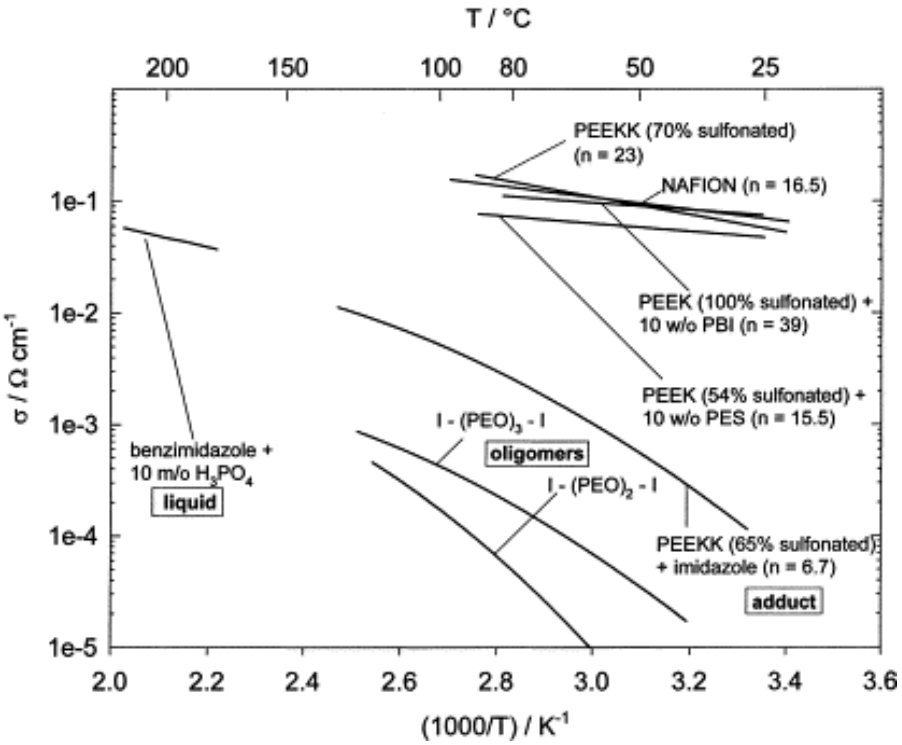

Figure 4. Proton conductivity of different fully hydrated acidic polymers, the liquid benzimidazole/H_3PO_4 system, and ethoxylated imidazole oligomers [10]

Despite its position as the benchmark PEM, Nafion® does have limitations. First, the proton conductivity is strongly dependant on the relative humidity. When the operating temperature is above 100°C, water is driven out of the system and this causes proton conductivity to drop dramatically. Second, fluorosulfonic acid PEMs are expensive, typically adding thousands of dollars to the cost of a PEMFC-powered car[9]. Third, methanol crossover limits the performance and utility of fluorosulfonic acid PEMs in direct-methanol fuel cells. Therefore, new cost-effective, methanol-compatible PEM materials are needed in which a high level of proton conductivity is maintained at elevated temperatures and low relative humidities.

The proposition by Kreuer et al of the potential utility of polymer membranes containing the imidazole functionality as an option in meeting the high-temperature membrane problem continues to be of interest. Liquid imidazolium salts and small molecule imidazole derivatives are not suitable, in themselves, as membranes in electrochemical devices because they are liquid and mobile. In 1997, Fuller and coworkers studied ionic liquid-polymer gel electrolytes and described ionic liquid/PVF_2 composites that are nonvolatile and are thermally stable. They

developed rubbery gel electrolytes that use ionic liquids and poly(vinylidene fluoride/hexafluoropropylene) copolymer, PVF_2/(HFP), and found that the ionic liquid-PVF_2(HFP) gels are freestanding and flexible and have conductivity levels between 1.1 and 5.8 mS/cm at room temperature. Since the ionic liquids and the PVF_2(HFP) are nonvolatile and thermally stable at temperatures up to 200°C, the gel can be operated successfully without degradation[11]. Thus, it was demonstrated that robust ion conductive membranes might be fabricated using PVF_2 as the host for ionic liquid salts.

B. PVF_2 and related copolymers

Polyvinylidene fluoride (PVF_2) is a semi-crystalline polymer with a relatively low melting point (160 - 170˚C), high purity, high mechanical strength. Like other fluoropolymers, it is substantially inert and it is resistant to most chemicals, solvents, weathering conditions, and high temperatures. Moreover, is easily purified, lower cost than fluorosulfonic acid polymers, and easy to process from solution or from a melt. PVF_2 is widely used in the chemical process industry[12] and in semiconductors,[13] wire and cables,[14] piping[15] and lithium batteries.[16]

An important property of PVF_2 is that it is ferroelectric.[17] When it is heated, subjected to an electric field to orient its molecular dipoles, and then cooled and allowed to recrystallize in the presence of an applied electric field, piezoelectric properties are induced within this material. Its glass transition temperature (T_g) is about -35°C; the material has a crystallinity of 50-60%.[18] In the crystalline state PVF_2 can arrange into at least three types of molecular conformations, TGTG, TTTT, and TTTGTTTG. Figure 5 illustrates theses conformers.

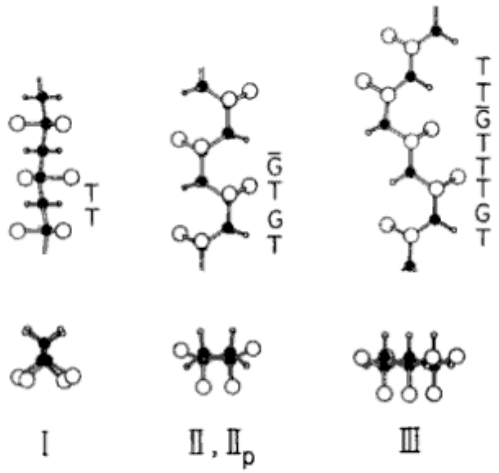

Figure 5. Conformers of PVF_2 [19]

Four crystalline modifications of PVF_2 are known: α, β, γ, and δ. In Figure 6, form I represents β type PVF_2, form II & II_p represent α and δ type, and form III represents γ type crystalline PVF_2. Crystal form I is generally prepared by stretching this material at room temperature. Form II is obtained by cooling from the melt at a moderate rate (e.g., 10-20°C/min or higher). The spherulites of Form III are obtained by slow cooling from the melt.

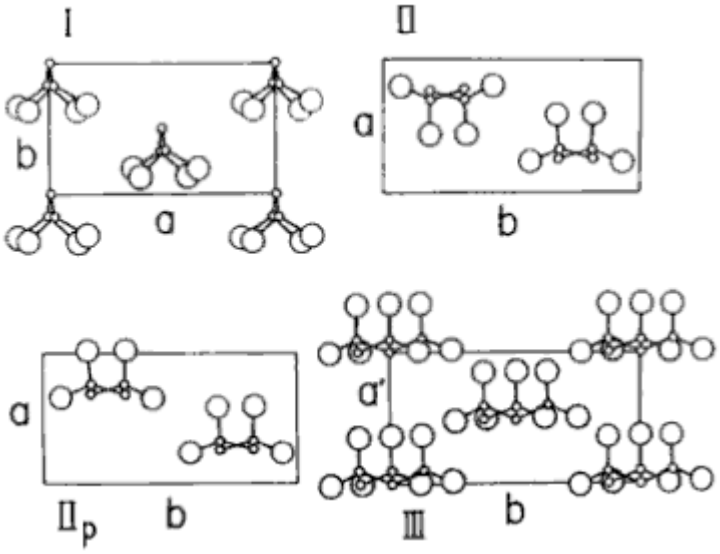

Figure 6. Crystal structure of four crystalline modifications of PVF_2[19]

PVF_2 is most often obtained as the alpha-phase material. The piezeoelectrically active form is the β-phase material. Copolymers of PVF_2 are typically less polar than pure PVF_2.

Because of the many favorable properties that PVF_2 possesses, the current work explores the use of this material (Kynar®301) and two copolymers thereof (Kynar®2801 and Kynar®7201) for use in the preparation of PVF_2/poly[(4(5)-VIm/VIm^+TFSI^-] composite films.

The structure of these polymers is depicted in Figure 7, below.

Kynar®301
Poly(vinylidene fluoride)

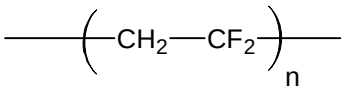

Kynar®2801
Copoly(vinylidene fluoride/hexafluoropropylene)

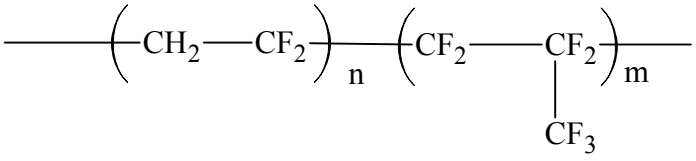

Kynar®7201
Copoly(vinylidene fluoride/tetrafluorethylene)

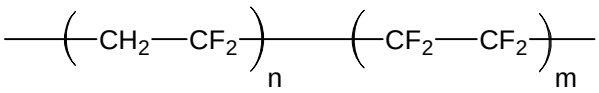

Figure 7. Structures of PVF_2 and PVF_2 copolymers

C. **Imidazole polymer systems**

Given that the present research is concerned with the use of imidazole containing polymers, this section gives a broad review of the literature on the use of the imidazole system as vehicle for proton exchange.

Imidazole is an aromatic heterocycle whose structure is shown in Figure 8. Kreuer et al.[20] were the first to propose that imidazole might be useful as a substitute for water at higher temperatures (150°C-250°C) in proton exchange fuel cell membranes.

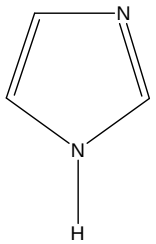

Figure 8. Molecular structure of 4(5)-vinylimidazole

Imidazole is an amphoteric base with a pK_a of 7 and, like water, can undergo autoprotolysis. It is a bidentate nucleophilic base that is strongly hydrogen bonded and can support proton transfer by the Grötthus mechanism[21,22] in which a concerted transfer of protons proceeds through a proximate chain of hydrogen-bonded molecules as shown in Figure 10.

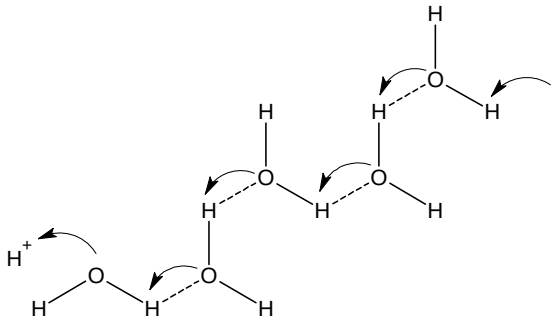

Figure 9. Grötthus mechanism of proton transport through water molecules

Water can transport protons by a Grötthus mechanism as shown in Figure 9. As reported by Kreuer, H-bonded sequences of imidazole molecules can also transport protons via this mechanism. The mechanism of movement of an excess proton though a sequence imidazole moieties by a Grötthus process is shown in Figure 10.

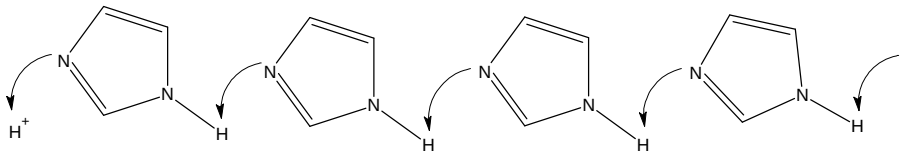

Figure 10. Grötthus mechanism of proton transport through imidazole molecules

The molecular weight of water is low and, in comparison to imidazole, its volatility is high, particularly at the temperatures encountered in fuel cell membranes. Kreuer employed imidazoles with flexible polyether tethers to study the contribution of proton mobility, proton transfer between imidazoles, and diffusion to proton transport. Scharfenberger, Kreuer and coworkers[23] synthesized proton-conducting imidazole polymers tethered to a polysiloxane backbone via flexible alky side-chains (spacer) and studied their utility as proton transporting media. Cyclic oligomers and open chain polysiloxanes with tethered imidazole moieties were also examined as proton solvents. They found that the polymers with the longest tethers had the highest proton conductivities. Furthermore, they reported that polymers with siloxane backbones were flexible and had a small repeat unit which can allow for high side-chain density. The

polysiloxanes and cyclic oligomers were stable up to at least 200°C and had a relatively high proton conductivity of around 1.5 x 10^{-3} Scm^{-1} at 160°C. Samples with long tethers have the lowest glass transition temperatures.

In related work, Pu, Meyer and Wegner studied the proton conductivity of poly[4(5)-vinylimidazole] blended with H_3PO_4 and H_2SO_4.[24] When the polymer was 100% protonated, the conductivity was characteristic of the acid itself. Furthermore, as can be seen in Figure 11, the conductivity of the blends increased as the temperature was increased. The level of conductivity when the molar ratio of acid to imidazole is high (X = 1.0 – 2.0) is 4-5 orders of magnitude greater than when the polymer is only fractionally protonated. In other words, poly[4(5)-VIm] doped with high levels of acid are essentially behaving as H_3PO_4or H_2SO_4 membranes. Pu and coworkers therefore postulated that proton conductivity in these blends could result from both proton hopping and polymer segmental movement. As the temperature approached and exceeded the glass transition temperature, segmental motion of the polymer increased, resulting in better conductivity. They also found that the conductivity of poly[4(5)-vinylimidazole] protonated with H_2SO_4 was higher than that of poly[4(5)-vinylimidazole] protonated with H_3PO_4. This was ostensibly because H_2SO_4 is a stronger acid than H_3PO_4.

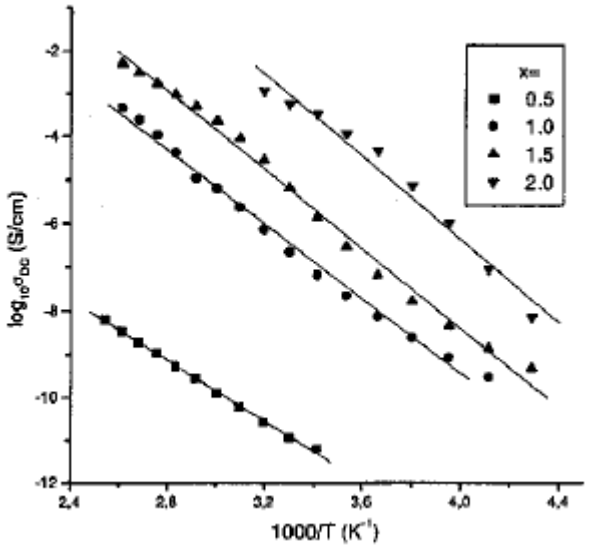

Figure 11. Temperature dependence of DC conductivity of poly[4(5)-vinylimidazole] blended with H_3PO_4 at various molar concentration ratios, X.[24]

Bozkurt and coworkers[25] also investigated the proton conductivity in poly(4-vinylimidazole) protonated with phosphoric acid. The number of moles of phosphoric acid per poly(4-vinylimidazole) repeat unit was varied between X = 0 and 2. They reported that blends are thermally stable up to 150°C and that their glass transition temperature is reduced as the molar concentration of phosphoric acid is increased. The conductivity reaches about 10^{-4} S/cm for the blends with 2 moles of phosphoric acid per poly(4-vinylimidazole) repeat unit. Figure 12 shows the log σ versus 1000/T for the two blends of poly(4-vinylimidazole) with H_3PO_4 and the pure polymer. The conductivity is lower in the pure polymer than that in the two blends with H_3PO_4. As the acid content is increased, the mechanism of proton transport is reported to change from Grötthus transport to proton movement through free acid with poly(4-vinylimidazole) merely serving as a support that is plastized by H_3PO_4 (a H_3PO_4 membrane in its essence). The authors of this work suggest that this change occurs because proton transfer between the phosphate units predominates when phosphoric acid has been added to the polymer.

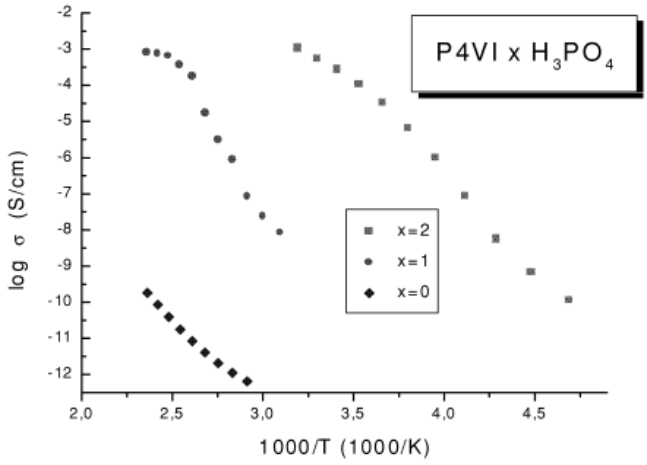

Figure 12. Temperature dependence of DC conductivities of poly(4-vinylimidazole) and the poly(4-vinylimidazole)–x H_3PO_4 blends [25]

Meilin Liu and coworkers[26] have studied triazole-containing PEMs. 1,2,3-triazole like imidazole is a multi-dentate nitrogen heterocycle that can potentially support proton transport by a Grötthus mechanism. The pK_a of the amine hydrogens in 1,2,3-triazole are pK_{a1}= 1.17, pK_{a2} = 9.26. The triazole is a stronger acid, in itself, than is imidazole. Given this greater acidity proton transport in neutral 1*H*-1,2,3-triazole could be expected to be significantly greater than that in neutral imidazole. Indeed, Liu found that 1*H*-1,2,3-triazole has a higher proton conductivity than

poly(4-vinylimidazole). The comparison of the conductivities between poly(4-vinyl-1H-1,2,3-triazole) and poly(4-vinylimidazole) is shown in Figure 13.

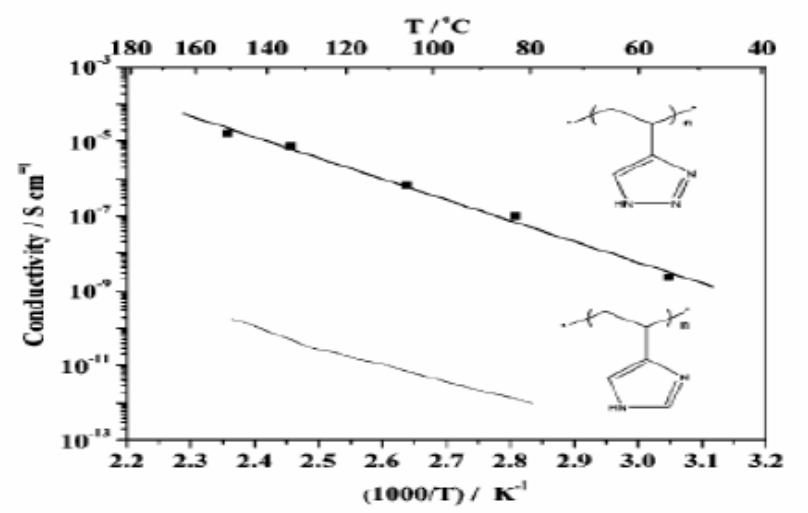

Figure 13. Proton conductivity of poly(4-vinyl-1H-1,2,3-triazole) and poly(4-vinylimidazole)[26]

In studies by Martinelli and coworkers[27], the physical properties of potential proton conducting membranes based on protic ionic liquids (ILs) were investigated as a function of IL/polymer ratios and temperature. The ionic liquid, N-ethylimidazolium bis(trifluoromethanesulfonyl)imide, EImTFSI, was incorporated into a matrix based on a poly(vinylidene fluoride) (PVF_2) copolymer. They found that the thermomechanical stability of the membranes was increased with increasing polymer content; however, conductivity decreased concomitantly, due to changes in the morphology of the membrane and interactions between the polymer matrix and the ionic liquid. They found the starting polymer matrix, PVF_2, has, predominantly, the polar crystalline structure, form III which is characterized by the polar $TTTG^-$ sequence in the unit cell of PVF_2. When temperature was increased but kept below the melting point of the membrane, crystalline form III was transformed to an amorphous phase. Increasing polymer content increases the glass transition temperature of the amorphous ionic liquid/PVF_2 phase in the membrane and has a subtle impact on the temperature dependence of the conductivity, presumably, due to geometrical confinement of the ionic liquid in the polymer matrix. Figure 14, displays the ionic conductivity of the three membranes and of the pure ionic liquid as a function of temperature. The inset shows the concentration dependence of the conductivity at room temperature.

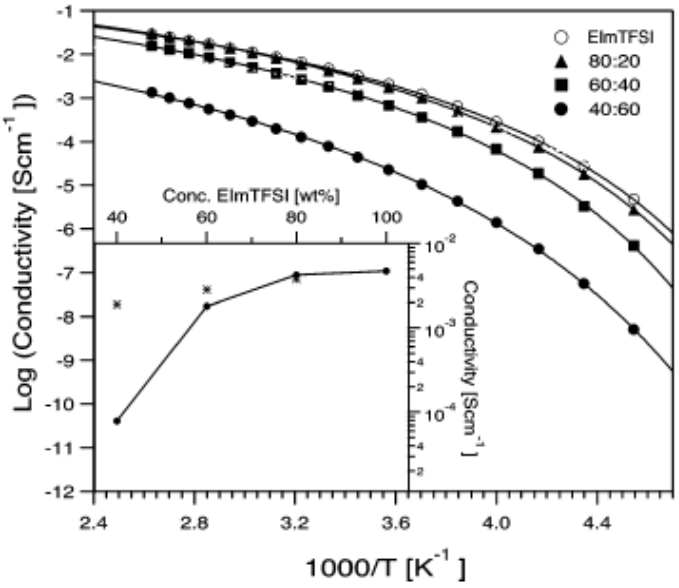

Figure 14. Ionic conductivity of PVF_2/EIm^+TFSI^- composite membranes[27]

In similar work, Fernicola and coworkers[28] showed that proton-conducting membranes, formed by incorporating Brønsted acid-base ionic liquids (ethylmethylimidazolium, methylimidazolium and methylpyrrolidinium) in a poly(vinylidenefluoride-co-hexafluoropropylene) polymer matrix, exhibit high thermally stability. However, the release of the ionic liquid (IL) component affects the long-term stability of the membranes. The authors proposed that the stability might be improved by incorporating ceramic fillers in the PVF_2/ionic liquid composites.

Masayoshi Watanabe and coworkers[29] characterized the ionic conductivity and proton conductivity under anhydrous conditions of a system comprised of imidazole (Im) and bis(trifluoromethanesulfonyl)imide (HTFSI) at various molar ratios of Im to HTFSI. High proton conductivity was observed in ionic liquid compositions comprised of imidazole that was fractionally protonated with HTFSI. The proton conductivity increased dramatically with increasing levels of HTFSI up to a mole fraction of about 0.1 and then decreased steadily as the mole fraction of HTFSI is increased beyond this point (See Figure 15). Direct current polarization measurements were employed to confirm proton conduction. Self-diffusion coefficients, measured by pulsed-gradient spin-echo NMR methods, indicated that fast proton exchange reactions between protonated imidazole cations and unprotonated imidazole molecules took place in the presence of excess imidazole. The process of proton conduction was assumed to

be a combination of Grötthus - and vehicle-type mechanisms. In the latter case movement of H_3O^+ is responsible for proton conduction.

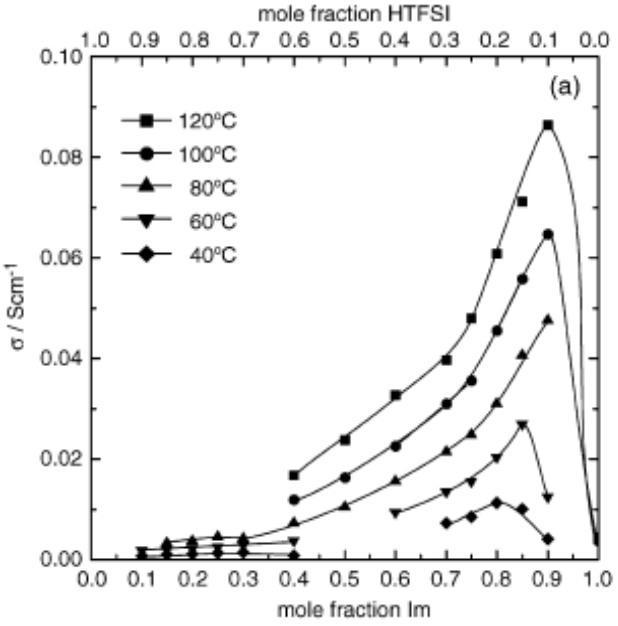

Figure 15. Ionic conductivity as a function of the mole fraction of imidazole (Im) in Im/*bis*(trifluoromethanesulfonyl)imide (HTFSI) mixtures [29]

D. Poly[4(5)-vinylimidazole]

Poly[4(5)-vinylimidazole], shown in Figure 16, exhibits close proximity and high volume density of imidazole groups. Accordingly, one might expect that proton conductivity by a Grötthus mechanism might be maximized in this polymer.

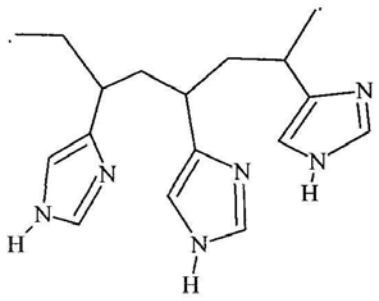

Figure 16. Poly[4(5)-vinylimidazole]

Films of poly[4(5)-vinylimidazole] are however brittle and difficult to fabricate as free-standing films. Moreover, poly[4(5)-VIm] is not stable to the chemical/oxidative environment of

an operating PEMFC. Wu and Smith[30] have mitigated these problems with the development of a new process for preparation of nanostructured composites of PVF_2 with PVIm/Im^+TFSI^-.

E. The work of Jinghang Wu

Wu formulated, fabricated and characterized PVF_2/poly[4(5)-vinylimidazole/imidazolium trifluoromethylsulfonylimide] composite films. In order to prepare composites of poly[4(5)-vinylimidazole] with PVF_2, it is necessary to dissolve the two polymers in a common solvent. However, given the solubility characteristics of poly[4(5)-vinylimidazole] this could not be achieved. Wu and Smith[30] discovered that fractional and full protonation with trifluoromethyl sulfonylimide enabled the preparation of homogeneous solutions of PVF_2 and poly[4(5)-VIm/VIm^+TFSI^-] in dimethylformamide. Given this discovery, Wu dissolved poly[4(5)-vinylimidazole] protonated with 50 mol% TFSI and poly(vinylidene fluoride)], PVF_2 in dimethylformamide (DMF) and cast films from these solutions. Films were dried and heat treated under differing conditions to obtain composites which were believed to have different PVF_2 crystallite sizes and morphologies. Composite films were prepared in which the ratio of Kynar® 301 PVF_2: PVIm was 3:1, 4:1 and 8:1, respectively. Wu also characterized the composite films by differential scanning calorimetry (DSC). His DSC thermograms displayed melting endotherms for PVF_2 in the 3/1, 4/1 and 8/1 composites at about 169 °C and a recrystallization exotherm peaking at about 125 °C. The melting and recrystallization temperatures of PVF_2 in the composites were analogous to those of pure PVF_2. The glass transition temperature of poly[4(5)-VIm] complexed with 50 mol% $TFSI^-$ was -30°C. The composite films doped with benzoyl peroxide (BPO) had more crystallinity than films without BPO. Incorporation of BPO apparently caused the % crystallinity of the 3/1 and 4/1 composite films to increase slightly and the crystallinity of the 8/1 composite films to increase substantially. Polarized optical microscopy was carried out to observe crystals in the composite films. Using a hot-stage on the microscope it was observed that PVF_2 crystals were molten at 200°C, revealing a dark field from amorphous poly[4(5)-VIm/VIm^+TFSI^-] phase. The background field became brighter when cooling to ambient temperature. Thermogravimetric analysis (TGA) established that the decomposition temperature of poly[4(5)-VIm/VIm^+TFSI^-] is 300°C and the temperature of decomposition of PVF_2 is 450°C. In addition, proton conductivity was measured at 80°C. The conductivity of the 4/1 PVF_2/poly[(4(5)-VIm/VIm^+TFSI^-] was slightly greater than that of the

3/1 composite film; the 8/1 composite film did not show any proton conductivity. Wu reported that at 80% relative humidity, conductivity of 0.05 S/cm, approaching that exhibited by Nafion® 112 (0.18 S/cm), was realized in a 4/1, PVF_2/poly[4(5)-VIm/VIm^+TFSI^-] composite film.

Based on the background information and Wu's work, described above, PVF_2//PVIm/$Im^+TFSI^-(4/1)_v$ composites were fabricated in which the mol% of TFSI was 15, 25, 35 and 50 mol%. In Wu's work, the crystal habit of the PVF_2 in the heated and non-heated films was not determined, and only one level of TFSI (50 mol%) was evaluated. In the present research, the crystal habit of PVF_2 and the morphology of PVF_2//PVIm/Im^+TFSI^- composites were studied by X-ray diffraction, DSC and solvent extraction.

II. Experimental

A. Materials

Urocanic acid (99%), dibenzoyl peroxide (BPO), and ammonium persulfate (98%) were obtained from Acros Organics. Trifluoromethanesulfonylimide (TFSI) (95%), N,N'-dimethylformamide (DMF) (99.8%), dimethylacetamide (DMAC), azobisisobutyronitrile (AIBN), 4,4-azobis(4-cyano valeric acid) (75%) were purchased from Sigma-Aldrich, Inc.. Benzene was purchased from EMD Chemicals Inc. Methanol was purchased from J.T. Baker. Ethyl alcohol (absolute anhydrous) was purchased through VWR, Bridgeport, NJ. Kynar® 301F poly(vinylidene fluoride), Kynar® 2801F copoly(vinylidene fluoride), Kynar® 7201F copoly(vinylidene fluoride) were obtained from Atochem North America, Inc.

B. Synthesis of 4(5)-vinylimidazole

4(5)-vinylimidazole was synthesized by decarboxylation of urocanic acid in accordance with the procedure published in Macromolecular Synthesis by Overberger et al.[31] Thus, 5 grams of anhydrous urocanic acid was placed into a short path distillation apparatus which was then immersed in a 230°C oil bath to effect decarboxylation of urocanic acid. The resulting 4(5)-vinylimidazole was refluxed under vacuum over a period of about four and a half hours. The crude 4(5)-vinylimidazole that was obtained was placed in a refrigerator overnight, and then held at room temperature for two hours to cause recrystallization. The purification of crude 4(5)-vinylimidazole was done by sublimation. Typically, 2 grams of 4(5)-vinylimidazole was placed in a sublimator, which was then immersed in a 70°C oil bath under a vacuum of (~0.5 x 10^{-3} torr). Over a period of about 4 hours pure white crystals formed on the cold finger of the sublimator. The yield of pure 4(5)-vinylimidazole was 1.63 grams (81%).

C. Synthesis of Poly4(5)-vinylimidazole

1) Polymerization of 4(5)-vinylimidazole in benzene solution initiated by azobisisobutylnitrile(AIBN)

Sublimed 4(5)-vinyl imidazole (1.5 g) and azobisisobutylnitrile (AIBN; 0.048 g) were dissolved in 10 ml benzene and placed into a pressure tube. The solution was purged with argon for 30 minutes and the pressure tube was capped with a crown cap. The tube was immersed in a 60°C water bath and held at this temperature for at least 24 hours. As the polymer formed, it precipitated out of solution because of its insolubility in

benzene. After the polymerization was completed, the tube was opened and benzene was decanted. Poly[4(5)-vinylimidazole], wet with benzene, was dissolved in methanol. Hexane was added to this methanol solution until the solution turned cloudy, and then a drop of methanol was added to clear the solution. This solution was added dropwise to a ~200 ml of acetone under constant stirring. The polymer was isolated by centrifugation. A yield of 1.57 g was obtained after drying at ambient temperature. Given that mass was in excess of 1.5g it is assumed that this polymer was not fully dried.

2) *Polymerization of 4(5)-vinylimidazole in ethanol/water solution initiated by 4,4-azobis(4-cyanovaleric acid)*

Sublimed 4(5)-vinyl imidazole (2 g) and recrystallized 4,4-azobis(4-cyanovaleric acid) (0.2 g) in 10ml ethanol/6ml distilled water were added to a pressure tube. The pressure tube was purged with argon gas for 30 minutes and then the tube was capped and immersed overnight in a 65°C water bath. After the polymerization, the tube was opened and the polymer solution appeared clear and viscous. Poly[4(5)-vinylimidazole] was precipitated from acetone by adding a few drops of hexane was added to the polymer solution. Poly[4(5)-vinylimidazole] (1.60 g) was collected by filtration and air-dried overnight.

D. PVF_2 Stock Solutions

1M trifluoromethylsulfonylimide (TFSI) stock solutions in DMF and DMAC were respectively prepared by diluting 2.67 grams of TFSI to 10 ml in a volumetric flask to volume. Solutions of Kynar®301F, Kynar®2801, and Kynar®7201 in DMF (15% polymer w/v) were simply prepared by dissolution of polymer (2 g) in 13.5 mL of solvent. Solutions of poly[4(5)-VIm/VIm^+TFSI^-], (Kynar®301F), and (Kynar®2801F in DMF (20% polymer w/v) were prepared by dissolving 30 grams of polymer in 140 ml of solvent. Solutions of Kynar®301F and Kynar®2801F in DMAC (15% polymer w/v) were prepared by dissolving 2 grams of polymer in 13.5 ml of solvent. Solutions of Kynar®301F and Kynar®2801F in formamide (20% polymer w/v) were prepared by dissolving 30 grams of PVF_2 into 140 ml of solvent.

E. **Poly[4(5)-vinylimidazole] solutions protonated with various mol% of trifluoromethylsulfonylimide (TFSI) in DMF**

1) *Solution of poly[4(5)-vinylimidazole] in DMF (15% polymer w/v) protonated with 15 mol% TFSI*

Poly[4(5)-vinylimidazole] **(Experimental Section IIC2)** (1.0 grams (0.01 mol)) was charged to a disposable test tube. 0.42g (0.0015 mol) of TFSI was added to the test tube along with 8.05 ml DMAC to yield a homogeneous solution of poly[4(5)-vinylimidazole/imidazolium TFSI] $(0.85/0.15)_M$.

2) *Solution of poly[4(5)-vinylimidazole] in DMF (15% polymer w/v protonated with 25 mol% TFSI*

The above 15 weight% poly[4(5)-vinylimidazole] solution, 0.5 ml, doped with 15 mol% TFSI was charged to a disposable test tube and 0.0108g of TFSI was added to yield a homogeneous solution of poly[4(5)-vinylimidazole/imidazolium TFSI] $(0.75/0.25)_M$.

3) *Solution of poly[4(5)-vinylimidazole] in DMF(15% polymer w/v) protonated with 35 mol% TFSI*

The above 15 weight% poly[4(5)-vinylimidazole] solution, 0.5 mL, doped with 15 mol% TFSI was charged to a disposable test tube. 0.0255g of TFSI was added to the test tube to yield a homogeneous solution of poly[4(5)-vinylimidazole/imidazolium TFSI] $(0.65/0.35)_M$.

4) *Solution of poly[4(5)-vinylimidazole] in DMF (15% polymer w/v) protonated with 50 mol% TFSI*

The above 15 weight% poly[4(5)-vinylimidazole] solution, 0.5mL, doped with 15 mol% TFSI was charged to a disposable test tube. 0.04755g of TFSI was added to the test tube to yield a homogeneous solution of poly[4(5)-vinylimidazole/imidazolium TFSI] $(0.5/0.5)_M$.

F. Poly[4(5)-vinylimidazole] solutions protonated with various mol% trifluoromethylsulfonylimide (TFSI) in DMAC

1) *Solution of poly[4(5)-vinylimidazole] in DMF (15% polymer w/v) protonated with 15 mol% TFSI*

Poly[4(5)-vinylimidazole] **(Experimental Section IIC2)** (1.0 grams (0.01 mol)) was charged to a disposable test tube. 0.42g (0.0015 mol) of TFSI was added to the test

tube along with 8.05 ml DMAC to yield a homogeneous solution of poly[4(5)-vinylimidazole/imidazolium] $(0.85/0.15)_M$.

2) *Solution of poly[4(5)-vinylimidazole] in DMF (15% polymer w/v protonated with 25 mol% TFSI*

The above 15 weight% poly[4(5)-vinylimidazole] solution, 0.5 mL, doped with 15 mol% TFSI was charged to a disposable test tube. 0.0108g of TFSI was added to the test tube to yield a homogeneous solution of poly[4(5)-vinylimidazole/imidazolium TFSI] $(0.75/0.25)_M$.

3) *Solution of poly[4(5)-vinylimidazole] in DMF(15% polymer w/v) protonated with 35 mol% TFSI*

The above 15 weight% poly[4(5)-vinylimidazole] solution, 0.5 mL, doped with 15 mol% TFSI was charged to a disposable test tube. 0.0255g of TFSI was added to the test tube to yield a homogeneous solution of poly[4(5)-vinylimidazole/imidazolium TFSI] $(0.65/0.35)_M$.

4) *Solution of poly[4(5)-vinylimidazole] in DMF (15% polymer w/v) protonated with 50 mol% TFSI*

The above 15 weight% poly[4(5)-vinylimidazole] solution, 0.5mL, doped with 15 mol% TFSI was charged to a disposable test tube. 0.04755g of TFSI was added to the test tube to yield a homogeneous solution of poly[4(5)-vinylimidazole/imidazolium TFSI] $(0.5/0.5)_M$.

G. PVF_2(Kynar®301F) /poly[(4(5)-VIm/VIm^+TFSI^-]$_{(4/1)V}$ composite films from DMF

1) *PVF_2(Kynar®301F)/poly[(4(5)-VIm/$VIm^+TFSI^-(0.85/0.15)_M]_{(4/1)V}$ composite films*

Four parts by volume of a 15 weight% solution of PVF_2 (Kynar®301F) in DMF were mixed with one part by volume of a 15 weight% solution of [poly 4(5)-vinylimidazole/imidazolium TFSI]$(0.85/0.15)_M$ in DMF . The mixed solution was cast into films on a 25 x 75 mm glass plate mounted on a perforated vacuum drawdown table which was covered with a sheet of 1024 bond paper. The gap of an adjustable drawdown wedge was set at 27 mil. After the film was dried at room temperature overnight, it was heated at 100°C for one hour to yield an opaque white film. This process was repeated to prepare several films. Two dried films were heated on a hot plate at 200 °C for 5 minutes under argon to yield films with increased transparency.

2) *PVF_2(Kynar®301F)/poly[(4(5)-VIm/VIm$^+$TFSI](4/1)$_V$ composite films doped with TFSI at 25, 35 and 50 mol%*

The above process was repeated to prepare [poly4(5)-vinylimidazole/ imidazolium-TFSI](0.75/0.25)$_M$, [poly4(5)-vinylimidazole/imidazolium-TFSI](0.65/0.35)$_M$ and [poly4(5)-vinylimidazole/imidazolium TFSI](0.5/0.5)$_M$ composite films. Films of the above compositions were prepared by a procedure analogous to that used to prepare the PVF_2//PVIm/Im$^+$ composites containing [poly4(5)-vinylimidazole/imidazolium TFSI](0.85/0.15)$_M$.

H. PVF_2(Kynar®301F)/poly[(4(5)-VIm/VIm$^+$TFSI$^-$]$_{(4/1)V}$ composite films from DMAC

1) *PVF_2(Kynar®301F)/poly[(4(5)-VIm/VIm$^+$TFSI$^-$(0.85/0.15)$_M$]$_{(4/1)V}$ composite films*

Four parts by volume of a 15 weight% solution of PVF_2 (Kynar®301F) in DMAC were mixed with one part by volume of a 15 weight% solution of [poly 4(5)-vinylimidazole/imidazolium TFSI] (0.85/0.15)$_M$ in DMAC. The mixed solution was cast into films on a 25 x 75 mm glass plate mounted on a perforated vacuum drawdown table which was covered with a sheet of 1024 bond paper. The gap of an adjustable drawdown wedge was set at 27 mil. After the film was dried at room temperature overnight, it was heated at 100°C for one hour to yield an opaque white film. This process was repeated to prepare several films. Two dried films were heated on a hot plate at 200°C for 5 minutes under argon to yield films with increased transparency.

2) *PVF_2(Kynar®301F)/poly[(4(5)-VIm/VIm$^+$TFSI](4/1)$_V$ composite films doped with TFSI at 25, 35 and 50 mol%*

The above process was repeated to prepare [poly4(5)-vinylimidazole / imidazolium TFSI](0.75/0.25)$_M$, [poly4(5)-vinylimidazole / imidazolium TFSI](0.65/0.35)$_M$ and [poly4(5)-vinylimidazole/imidazolium TFSI](0.5/0.5)$_M$ composite films. Films of the above compositions were prepared by an analogue procedure to that used to prepare the (4/1) with 10 mol% TFSI composite.

3) *PVF_2(Kynar®2801F)/poly[(4(5)-VIm/VIm$^+$TFSI$^-$(15, 25, 35, 50mol% TFSI]$_{(4/1)V}$ composite films from DMAC*

Films with various levels of protonation of PVIm with TFSI (15, 25, 35 and 50 mol%) were prepared. PVF_2 (Kynar®2801F) in DMAC solution was added to the various PVIm/Im$^+$TFSI$^-$ DMAC solutions, respectively. The volume ratio of PVF_2 and

PVIm/Im^+TFSI^- was 4 to1. After all the composite films were cast, they were annealed on the hot plate in a glove box filled with Ar gas. The annealing procedure is given below. It took 30 minutes for the hot plate to heat up to the desired temperature. The films were then heated at 200 °C for another 30 minutes. After heating, cooling down to room temperature took about 60 minutes.

4) *PVF_2(Kynar®7201F)/poly[(4(5)-VIm/VIm^+TFSI(15, 25, 35, 50mol% TFSI]$_{(4/1)V}$ composite films from DMAC*

Films with various levels of protonation of PVIm with TFSI (15, 25, 35 and 50 mol%) were prepared. PVF_2 (Kynar®7201F) in DMAC solution was added to the various PVIm/Im^+TFSI^- DMAC solutions, respectively. The volume ratio of PVF_2 and PVIm/Im^+TFSI^- was 4 to1. After all the composite films were cast, they were annealed on the hot plate in a glove box filled with Ar gas. The annealing procedure is given below. It took 30 minutes for the hot plate to heat up to the desired temperature. The films were then heated at 200°C for another 30 minutes. After heating, cooling down to room temperature took about 60 minutes.

I. Characterization of the composite films

1) Differential Scanning Calorimetry (DSC)

DSC analysis was carried out under nitrogen on a Perkin Elmer Diamond DSC. Sample pans were heated and cooled at a rate of 20°C/min. All the samples were subjected to two heating and cooling cycles. Pure PVF_2 and films with different polymer compositions were evaluated before and after annealing at 200°C.

PVF_2 is a semicrystalline polymer. A typical protocol for the DSC analyses was to first ramp to 200°C, then cool to -70°C at a rate of 20°C/minute. Thus, the first scan was completed. This cycle was repeated until two DSC traces overlapped. The sample was then ramped to 200°C at a rate of 20°C/minute and cooled to -70°C at a rate of 20°C/minute. The analysis was thus a 7-step process.

Step 1 - Heat from 30°C to 100°C at 20°C/min

Step 2 - Hold for 2 min at 100°C

Step 3 - Cool from 100°C to -70°C at 20°C/min

Step 4 - Heat from -70°C to 200°C at 20°C/min

Step 5 - Cool from 200°C to -70°C at 20°C/min

Step 6 - Heat from -70°C to 200°C at 20°C/min

Step 7 - Heat from 200°C to -70°C at 20°C/min

PVF_2(Kynar®301)/poly[4(5)-VIm/VIm^+TFSI^-] composite films from dimethylacetamide (DMAC) were prepared and analyzed in an analogous manner. The composition of these films is listed below.

- PVF_2/poly[4(5)-VIm/VIm^+TFSI^-] (15mol%) $(4/1)_v$
- PVF_2/poly[4(5)-VIm/VIm^+TFSI^-] (25mol%) $(4/1)_v$
- PVF_2/poly[4(5)-VIm/VIm^+TFSI^-] (35mol%) $(4/1)_v$
- PVF_2/poly[4(5)-VIm/VIm^+TFSI^-] (50mol%) $(4/1)_v$

Two sets of films identified as "non-heated and heated" were analyzed for each composition. The non-heated films were dried at 50˚C on a hot plate overnight, and then were heated at 100˚C for 30 minutes in air. Heated films were obtained by heating at 200˚C for 5 minutes, and then cooling down to room temperature.

2) X-ray Diffraction

X-ray diffraction patterns were obtained on the above materials by Dr. Surendra K Gupta using a Rigaku DMAX-II B powder diffractometer with Cu Kα radiation (40 kV, 35 mA). Patterns were analyzed using MDI Jade 6 software with the ICDD PDF-4+ database. Films with the four different dopant levels, PVF_2 (Kynar®301F)/poly[4(5)-vinylimidazole] doped at 15, 25, 35 and 50 mol% TFSI were analyzed both before and after heating at 200 °C. All the films were glued to glass slides with LOCTITE glue.

3) Wide Angle X-ray Scattering (WAXS) at the Brookhaven Synchrotron

Crystallographic analysis for a set of films cast from DMAC and a sister set cast from DMF was sent to Dr. Peggy Cebe at Tufts University. X-ray diffraction spectra of composite films from DMF and DMAC were obtained on the synchrotron at Brookhaven. The PVF_2 (Kynar®301)/poly[4(5)-VIm/VIm^+TFSI^-] composite films from DMAC and DMF were doped with 15 and 35 mol% TFSI. All the compositions before and after heating to 200°C were studied. Each set of films was measured both free-standing and Kapton® mounted.

4) Extraction by water or water/ethanol mixture of PVF_2/poly[(4(5)-VIm/VIm^+TFSI^-] composite films

Water extraction of PVF_2/poly[(4(5)-VIm/VIm^+TFSI^-] composite films was carried out, in accordance with the following protocol. The initial weight of each composite film was recorded. Then all of the films were immersed in distilled water for 24-48 hours at ambient temperature. After immersion, the films were removed from the distilled water and air-dried for two weeks. Subsequently, they were heated at 70°C for four hours until they dried to constant weight. The difference in the weight of the initial film and the film after water extraction and drying was recorded as the mass of extracted materials. Water/ethanol extraction of PVF_2/poly[(4(5)-VIm/VIm^+TFSI^-] composite films was carried out with an analogous protocol. Each of the films that had been subjected to extraction with distilled water was soaked in ethanol/water solution for one day at ambient temperature. After extraction, the films were dried in air for one hour and then they were heated at 70°C for one hour to dry to constant weight. The difference in the weight of the initial film and the film after water extraction and drying is the mass of extracted material. Evaluation for percent of mass extracted from the composite films follows the equation below:

$$\%\ \text{mass extracted} = \frac{(\text{pre-soaked sample - dried sample})}{\text{pre-soaked sample}} \times 100\%$$

5) Viscometry

The viscosity of a dilute polymer solution can be used to determine the polymer's molecular weight. Basically, the solution viscosity relates to the size of polymer molecules. The procedure used to evaluate viscosity is that published by Cannon.[32] Thus, the efflux time (t) was measured for a specified volume of polymer solution to flow through the capillary tube. This time was compared with the time (t_0) required for pure solvent to pass through the viscometer. From t, t_0 and the solute concentration, the relative, specific, and reduced viscosities of a polymer solution can be determined using the following equations[33]:

Relative viscosity $\eta_r = \eta/n_0 = t/t_0$

Specific viscosity $\eta_{sp} = \eta_r - 1$

Reduced viscosity $\eta_{red} = \eta_{sp}/c$

The intrinsic viscosity is defined as $[\eta] = \eta_{red(c \to 0)}$, where c is the concentration of the polymer solution. The unit of concentration c is grams per milliliter. Intrinsic viscosity can be determined by extrapolating a plot of η_{red} vs. c. This intrinsic viscosity can be used to determine the molecular weight by using the Mark-Houwink-Sakurada equation: $[\eta] = K [\overline{M}_v]^a$, where the range of a is between 0.5 and 0.8.

A Cannon-Ubbehohde viscometer (size 75) was cleaned with hot sulfuric acid mixed with nochromix® solution in order to make sure the capillary tube was unobstructed. The visometric parameters $\eta_{r,}$ η_{sp} and η_{red} were evaluated under conditions of isoionic dilution for the PVIm polymerized in benzene and in ethanol/H_2O. Thus, 0.25 grams of PVIm were diluted with 0.5M KCl in methanol/$H_2O(1/1)_v$ in a 10ml-volumetric flask. A series of dilutions were then made using the KCl in methanol/water mixture. This was done to maintain constant ionic strength for all solutions. The series of diluted solutions had concentrations of 2.5, 1.25, 0.625, 0.5, 0.25 0.20, 0.15, 0.08 and 0.05 g/dL. The viscometer was placed into water bath at a temperature of 25˚C for about 15-20 minutes to equilibrate the temperature of viscometer at 25˚C. The Ubbeldode viscometer was used to measure the flow time of the solvent. At high dilution, gegenions that are not covalently bound to the polymer backbone can diffuse away from the polyion without isoionic dilution (maintaining constant ionic strength), this results in deshielding of positive charged Im^+ residues on the polymer chain. The resulting charge repulsion expands the dimension of the polymer coil and leads to an increase in hydrodynamic radius and viscosity.

The viscosity data for poly[4(5)-vinylimidazole] polymerized in benzene using AIBN and in ethanol/water using 4,4-azobis(4-cyanovaleric acid) are presented in Figure 17 as reduced viscosity, η_{red}, vs. mass concentration of polymer, c. The equations for the two straight lines in Figure 17 are given below. The y-intercept of each line gives the intrinsic viscosity of each sample.

PVIm (from benzene)	PVIm (from ethanol/H_2O)
y = 1188.2x + 42.203	y = 196.64x + 15.591
[η] = 42.203 mL/g	[η] = 15.591 mL/g

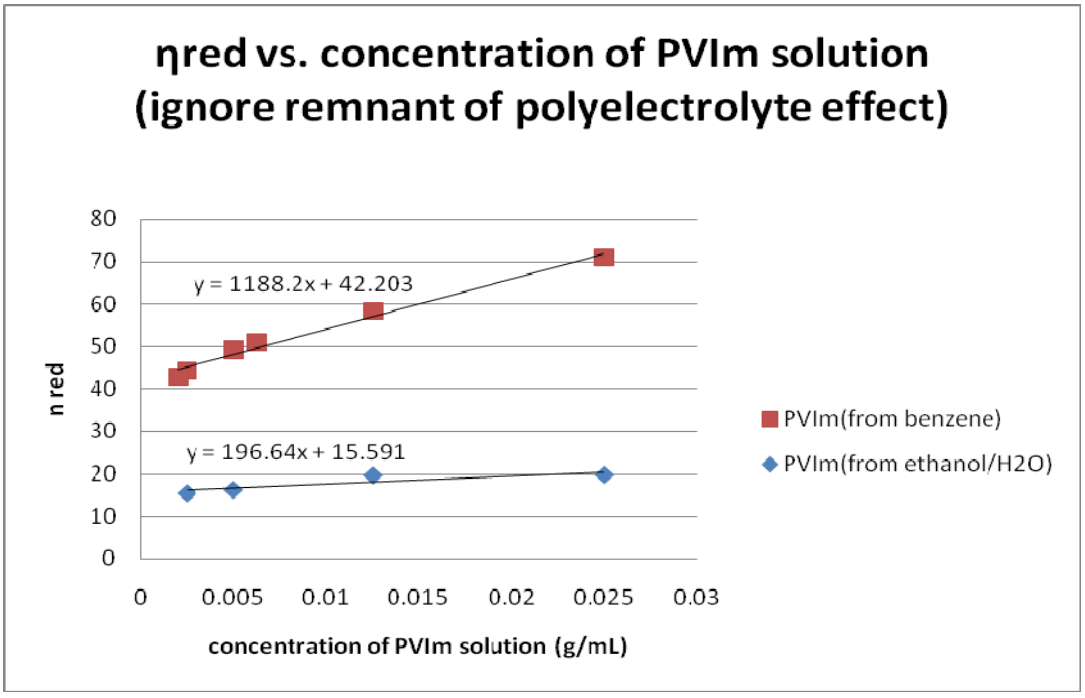

Figure 17. Reduced viscosity-concentration curve for a PVIm from benzene and ethanol/water

III. Results and Discussion

A. *Fabrication of PVF_2//PVIm/Im^+TFSI^- composite films*

In the present research, the structure, morphology, and composition of poly(vinylidene fluoride)/poly[4(5)-vinylimidazole/imidazolium trifluoromethylsulfonylimide] composites (PVF_2//PVIm/Im^+TFSI^-) have been examined.

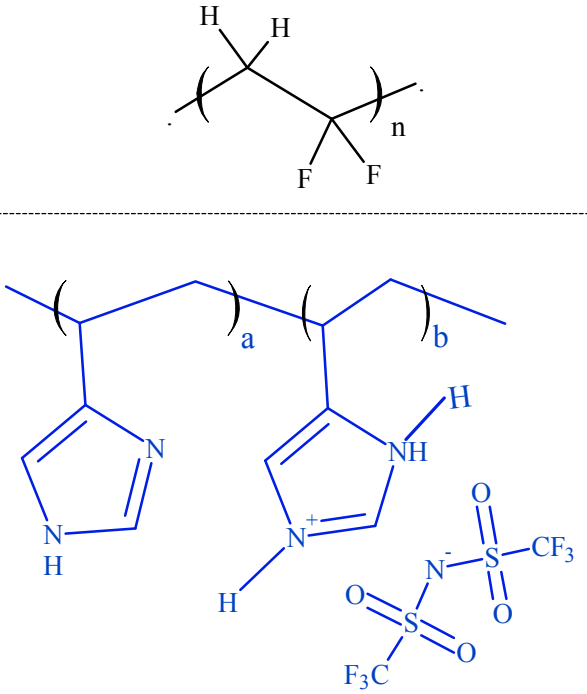

Figure 18. Structure of PVF_2/poly[4(5)-VIm/VIm^+TFSI^-]

This work builds on previous studies by Wu[30] in which PVF_2/PVIm/Im^+TFSI^- composites were prepared and their potential as proton-conductive membranes was explored. In that work, poly[4(5)-VIm] was protonated with 50 mol% TFSI, dissolved in DMF, and the resultant PVF_2//PVIm/Im^+TFSI^- solution was mixed with DMF solutions of PVF_2. Subsequently, films were cast from these mixed DMF solutions and dried and heated under differing conditions to obtain composites of different composition [$(3/1)_v$, $(4/1)_v$ and $(8/1)_v$, respectively], morphology, and, apparent PVF_2 crystallite size. The proton conductivity, at 80°C and 80% RH, of the PVF_2//PVIm/$Im^+TFSI^-_{(4//1)v}$ composite films were comparable to those of the PVF_2//PVIm/$Im^+TFSI^-_{(3//1)v}$ composite films. The proton conductivity of the PVF_2//PVIm/$Im^+TFSI^-_{(8//1)v}$ composite film was negligible. The PVF_2 composites were characterized by DSC and hot stage microscopy.

Building on this work, Wu's procedure for fabrication of PVF_2//PVIm/$Im^+TFSI^-_{(4/1)v}$ composites was repeated, varying the level of protonation with TFSI. Most importantly, a more quantitative evaluation of the crystallinity of the PVF_2 phase was undertaken. PVF_2//PVIm/Im^+ composite films were prepared and studied in which the mass fraction of PVF_2/PVIm was held constant at 4/1. The fraction of protonated imidazole residues was varied between 15 and 50 mol% TFSI. Films were cast from both DMF and DMAC and were characterized as cast at ambient temperature, drying at 100°C or less, and after heating to 200°C. In order to understand the PVF_2 crystal habit, α, β or δ,[19] X-ray diffraction studies were carried out by this author in Dr. Surendra Gupta's lab here at RIT and by Dr. Peggy Cebe (Tufts University) on the synchrotron at the Brookhaven National Laboratory. Percent crystallinity was evaluated by determination of the relative area under the fusion endotherms in DSC traces. T_m values appeared to be somewhat correlated with the PVF_2 crystal habit. Composite films were extracted with H_2O or H_2O/ethanol and the extractability of the PVIm/Im^+ component (% extractables) was interpreted, in part, as a reflection of the intimacy of the mixture.

In the following paragraphs, the results of experiments evaluating: 1) PVF_2 crystal habit by X-ray diffraction , 2) % crystallinity and melting characteristics by thermal analysis, and 3) extractability of the PVIm/Im^+ are presented. In the conclusion section, speculation is offered that renders an overall construct for the morphology of PVF_2//PVIm/Im^+ composite films

B. Characterization of the composite films

1) <u>X-ray diffraction studies</u>

Wide Angle X-ray Scattering (WAXS) at RIT

Figure 19 displays X-ray diffraction traces of a set of PVF_2//PVIm/Im^+ composite films cast from DMAC (identified as 301P-50, 301P-35, 301P-25, 301P-15 and 301P-50AN, 301P-35AN, 301P-25AN, 301P-15AN) wherein the level of protonation with TFSI was 50, 35, 25 and 15 mol%, respectively. AN is indicative of the fact that the film had been heated to 200˚C. One can see that the respective traces for the 301P 50, 35, 25 and 15 set and the 301P50-AN, 301P-35AN, 301P-25AN, 301P-15AN set are very similar. One also sees that the peaks in the 301P50-AN, 301P-35AN, 301P-25AN, 301P-15AN set are sharper and more distinct.

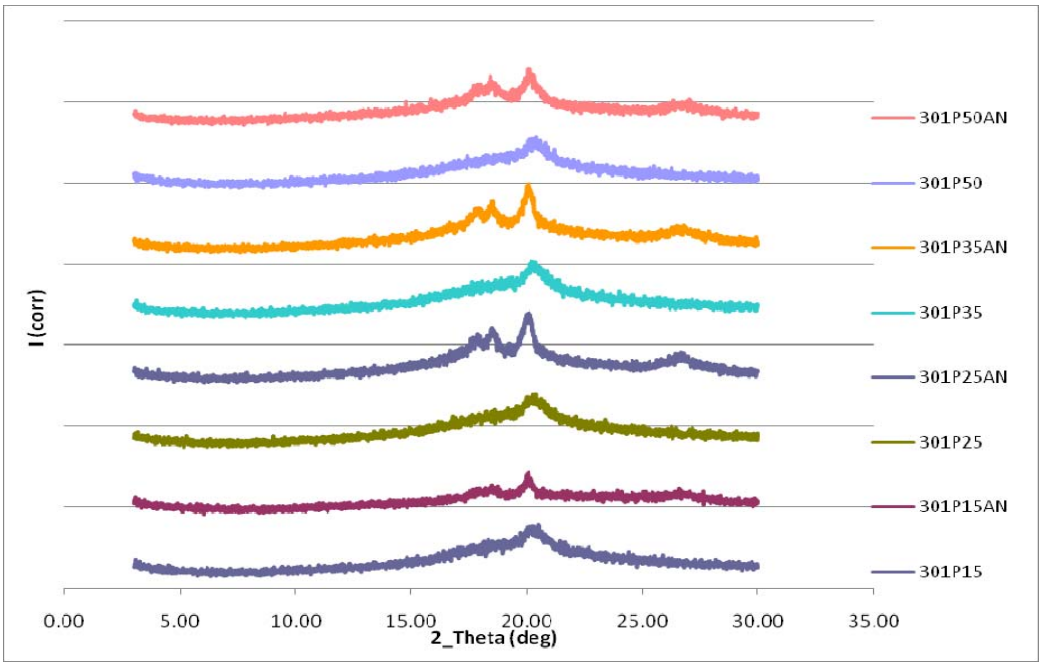

Figure 19. X-ray diffraction traces (spectra) of PVF_2/PVIm-Im^+ composite films cast from DMAC

The films in the AN set are physically stronger and, as shown in Figure 20, are translucent to transparent in appearance. The relative clarity or lack thereof, may be indicative of smaller crystallite size in the heated films than in the non-heated films. Indeed, it was suggested by Wu as the reason why heated films were substantially more transparent than the as-cast non-heated films. The PVIm/Im^+ is apparently acting as a nucleating agent for PVF_2 crystallization. The clarity is increased as the fraction of protonation is increased from 15 to 25, to 35, to 50 mol% TFSI.

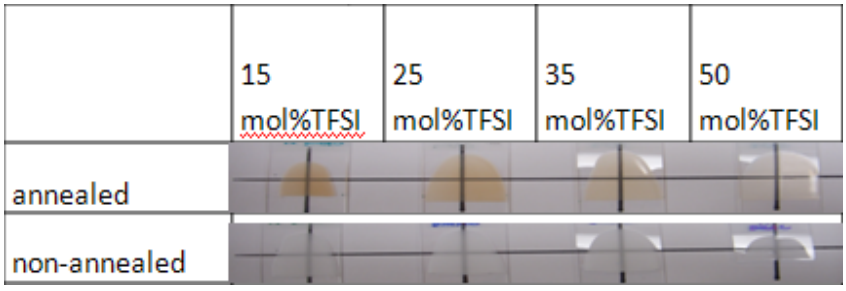

Figure 20. PVF_2/PVIm-Im^+TFSI^- composite films cast from DMAC

Figure 20 also shows some discoloration in each of the heated composite films. The discoloration is greatest in the 15mol% TFSI composite film, somewhat less in the 25mol% TFSI film, and only slight in the 35mol% TFSI and 50 mol% TFSI films. The reduced discoloration

with increasing TFSI content is indicative of increased thermal stability with higher levels of TFSI.

In order to obtain better crystallographic analysis, the set of films described above and a sister set cast from DMF were sent to Dr. Peggy Cebe at Tufts University. X-ray diffraction spectra of these composite films from DMF and DMAC were taken on the synchrotron at Brookhaven. Figure 21a shows the X-ray diffraction spectrum for a control film of PVF_2 (Kynar®301F), cast from DMF at ambient temperature and dried at 100˚C. The spectrum exhibits a predominant peak at 2θ = 18 degrees that can be attributed to β-phase PVF_2 crystals.[34] When this homopolymer film was heated to 200 ˚C and cooled to room temperature, the X-ray diffraction pattern, shown in Figure 21b, was obtained. It clearly shows a transformation from β-phase crystals to α-phase crystals that exhibit a multiplicity of peaks at 2θ = 12, 16.5, 17, 24 and 30 degrees.

Figure 21a

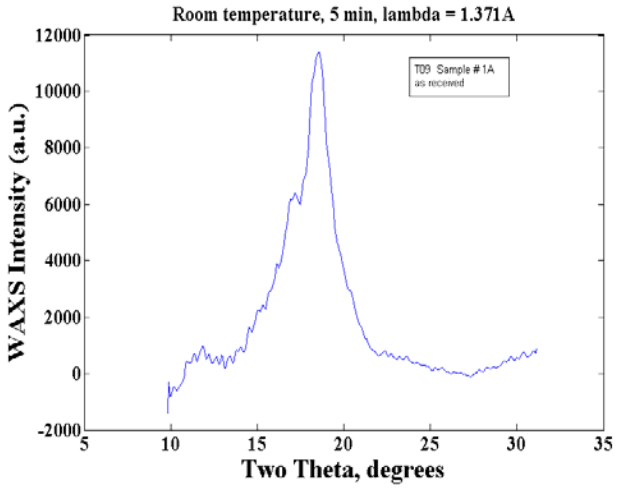

Figure 21a X-ray diffraction spectrum of β-phase PVF_2 cast from DMF at ambient temperature and dried at 100˚C

Figure 21b

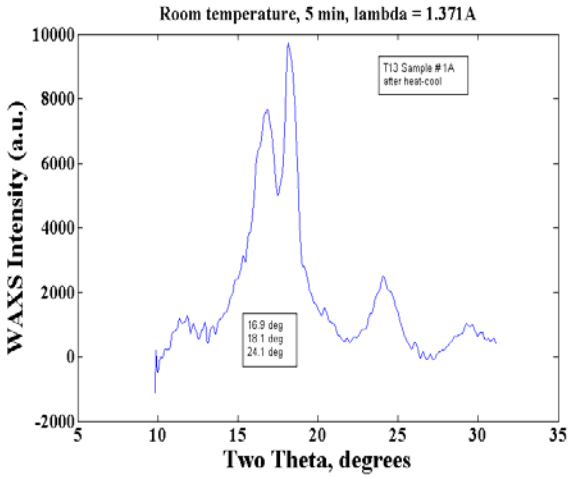

Figure 21b α-phase PVF_2 cast from DMF at ambient temperature and dried at 100 ˚C and annealed at 200˚C

Figures 22a and 23a show the X-ray diffraction spectra for composite films of PVF_2//PVIm/Im^+/$TFSI^-$ $(85/15)_M$ and $(65/35)_M$, cast from DMF at ambient temperature and dried at 100˚C. The spectra exhibit a predominant peak, like that in the control, that can be attributed to β-phase PVF_2 crystals.[34]

Figure 22a

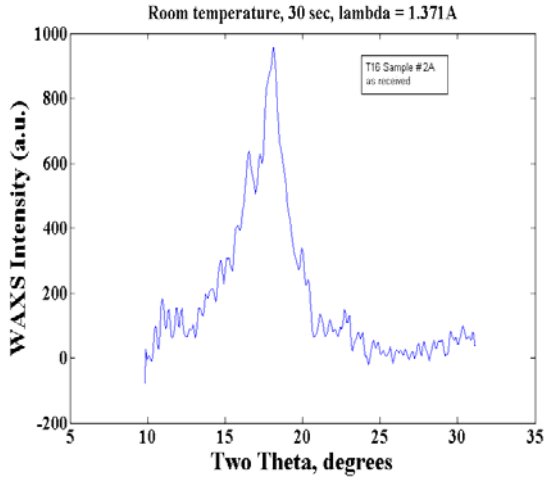

Figure 22a In the composite film that gave β-phase X-ray diffraction spectrum shown in Figure 22a. Poly[4(5)-VIm] was protonated with 15 mol% TFSI, dissolved in DMF. Cast from DMF at ambient temperature and dried at 100˚C

Figure 22b

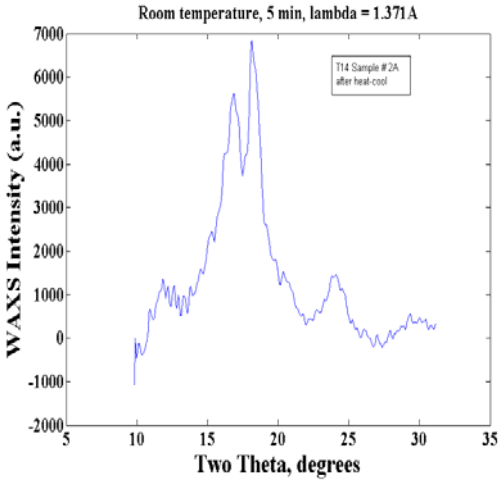

Figure 22b In the composite film that gave α-phase X-ray diffraction spectrum shown in Figure 22b. α-phase Poly[4(5)-VIm] was protonated with 15 mol% TFSI, dissolved in DMF. Cast from DMF at ambient temperature and dried at 100˚C and annealed at 200˚C

Figure 23a

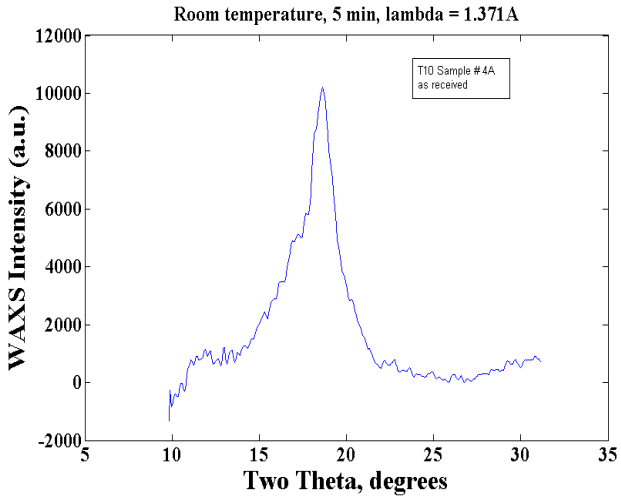

Figure 23a β-phase Poly[4(5)-VIm] was protonated with 35 mol% TFSI, dissolved in DMF. Cast from DMF at ambient temperature and dried at 100˚C

Figure 23b

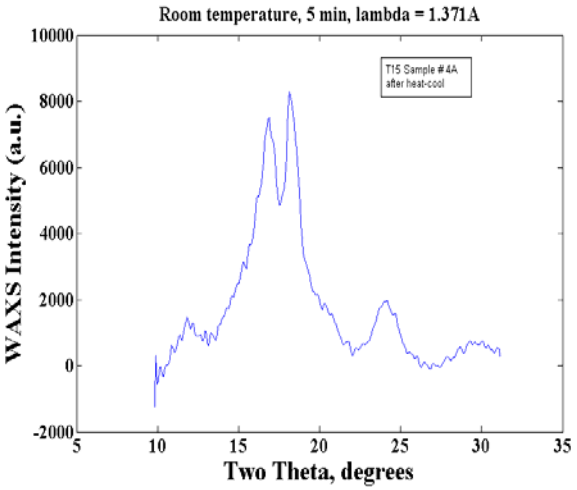

Figure 23b α-phase Poly[4(5)-VIm] was protonated with 35 mol% TFSI, dissolved in DMF. Cast from DMF at ambient temperature and dried at 100˚C and annealed at 200˚C

When these composite films were heated to 200˚C and cooled to room temperature, the X-ray diffraction patterns, shown in Figures 22b and 23b were obtained. As with the PVF_2 control film, after heating to 200˚C and rapid cooling, they clearly show a transformation from β-phase crystals to α-phase crystals that exhibit a multiplicity of peaks at 2θ = 12, 16.5, 17, 24 and 30 degrees.

Control and composite films cast from DMAC exhibited X-ray diffraction patterns analogous to those observed for films cast from DMF. Figures 24a, 25a and 26a show that β-phase crystals were obtained in films cast at ambient temperatures and dried at < 100˚C. Figures 24b, 25b and 26b show films, after heating to 200˚C, wherein a transformation from β-phase crystals to α-phase crystals has occurred.

Figure 24a

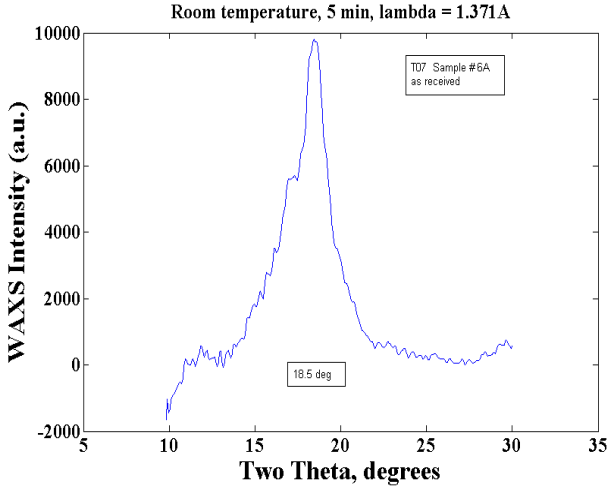

Figure 24a β-phase PVF_2 cast from DMAC at ambient temperature and dried at 100˚C

Figure 24b

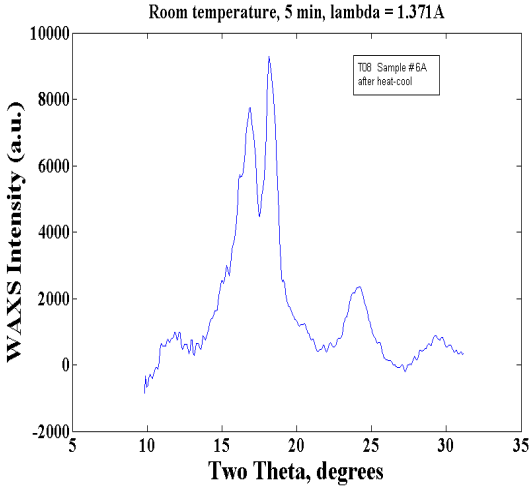

Figure 24b α-phase PVF_2 cast from DMAC at ambient temperature and dried at 100˚C and annealed at 200˚C

Figure 25a

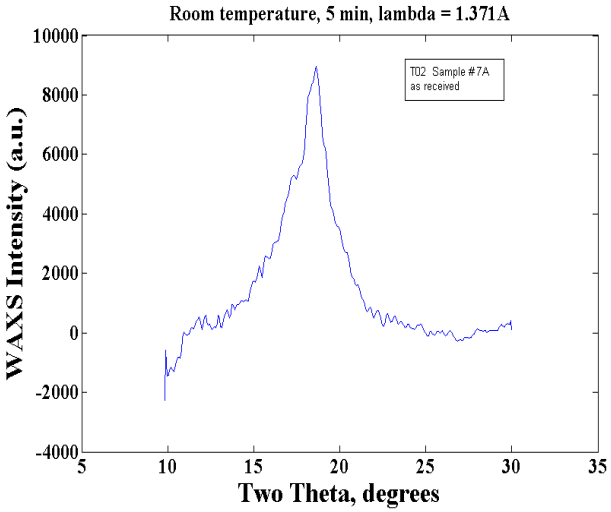

Figure 25a β-phase Poly[4(5)-VIm] was protonated with 15 mol% TFSI, dissolved in DMAC. Cast from DMAC at ambient temperature and dried at 100˚C

Figure 25b

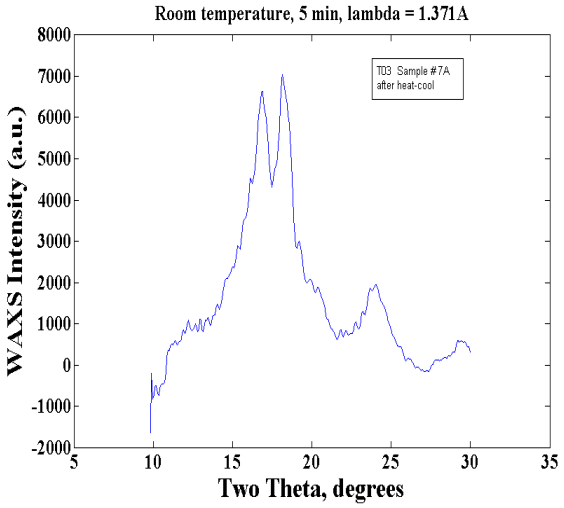

Figure 25b α-phase Poly[4(5)-VIm] was protonated with 15 mol% TFSI, dissolved in DMAC. Cast from DMAC at ambient temperature and dried at 100˚C and annealed at 200˚C

Figure 26a

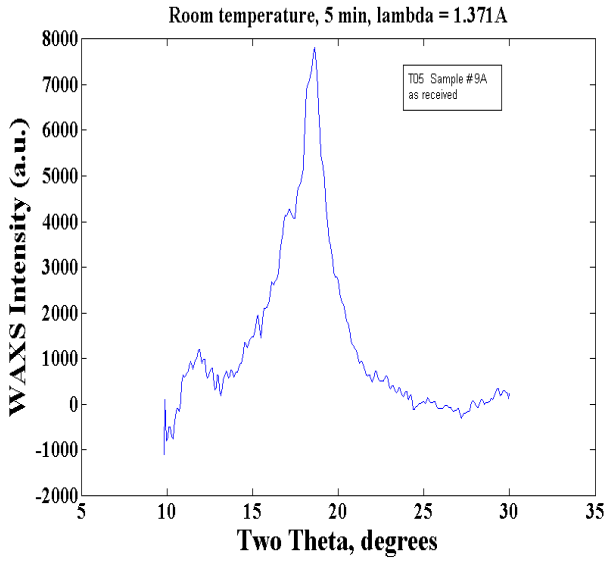

Figure 26a β-phase Poly[4(5)-VIm] was protonated with 35 mol% TFSI, dissolved in DMAC. Cast from DMF at ambient temperature and dried at 100˚C

Figure 26b

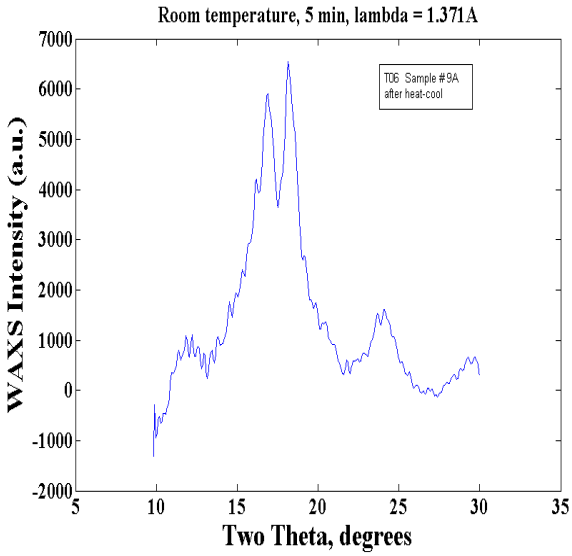

Figure 26b α-phase Poly[4(5)-VIm] was protonated with 35 mol% TFSI, dissolved in DMAC. Cast from DMF at ambient temperature and dried at 100˚C and annealed at 200˚C

The literature reports that β and γ-phase[35, 36] PVF_2 can be obtained when the polymer is cast from polar aprotic solvents like DMF and DMAC. It has also been reported that because of its faster crystallization rate at higher temperatures (110-150˚C),[37] α-phase PVF_2 is obtained when the polymer is rapidly cooled from the melt. On the other hand, β-phase crystallizes below 80˚C.[37] In PVF_2/PMMA blends, it has been reported that crystallization from the melt to β-phase is favored.[38] It is therefore perhaps of some note that PVIm//Im^+TFSI^- has no significant influence on the crystal habit of PVF_2.

The scheme shown in Figure 27 depicts the process for obtaining β-phase crystals from solution and the transformation to α-phase that is observed without respect to whether the solvent was DMF or DMAC and without respect to whether the material being processed was pure PVF_2 or a blend of PVF_2 and PVIm//Im^+TFSI^-. The % protonation with TFSI also has no apparent effect on the crystal habit of PVF_2.

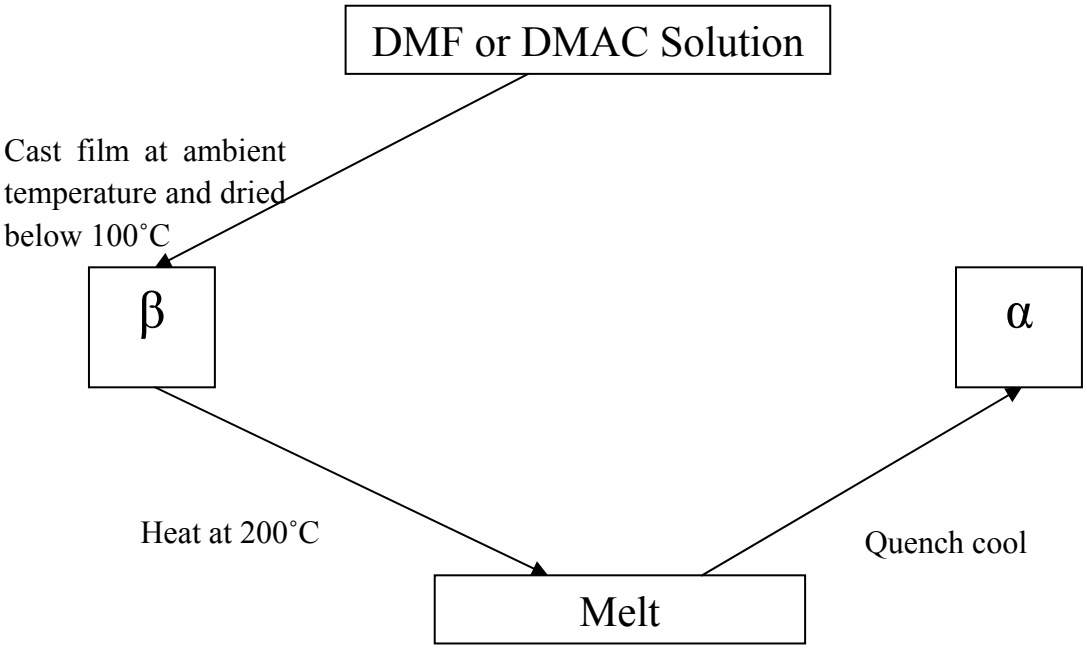

Figure 27. Transformation between the two main phases of PVF_2

Summarizing what has been learned in the course of the present X-ray diffraction analysis, it has been determined that PVF_2 films cast from DMF and DMAC, at ambient temperature and dried at temperatures below 100˚C, give membranes in which PVF_2 crystallites adopt a β-phase

crystal habit. Heating these films to 200˚C and rapidly cooling to ambient temperature results in a transformation of the PVF_2 crystallites to α-phase. PVF_2 homopolymer films cast from DMF or DMAC are white and substantially opaque (non-transparent). It seems that the size of PVF_2 spherulites is large and scattering of light makes the film appear opaque. When the PVF_2 film was heated at 200˚C and cooled to room temperature, α-phase crystals were obtained, however, the film remains white and substantially opaque in appearance. When the composite films of PVF_2 and $PVIm/Im^+$ protonated with 15, 25, 35 and 50 mol% TFSI were cast at ambient temperature and dried at 100˚C, β-phase PVF_2 was also obtained and the PVF_2 was transformed from β-phase to α-phase on heating to 200˚C and rapidly cooling to room temperature. However, in the composite films quenched from the melt, there was significant transparency in the films. The films with 15 mol% of TFSI were the least transparent. The films with 25 mol% of TFSI and 35 mol% of TFSI were increasingly transparent, and the film with 50 mol% TFSI was almost clear. It seems that $PVIm/Im^+TFSI^-$ serves as a nucleating agent and that at higher levels of protonation with TFSI, $PVIm/Im^+$ may be more miscible with the amorphous phase of PVF_2.

2) Thermal analysis of PVF_2//$PVIm/Im^+$ composites

a. DSC analysis protocol

PVF_2 control films and composites with $PVIm/Im^+TFSI^-$ containing 15, 25, 35 and 50 mol% TFSI and cast from DMF and DMAC were also studied by DSC. Two cycles were run heating at a rate of 20˚C/min. In the first cycle, all the films had not been previously heated above 100˚C. During the first heating cycle, samples were heated to 200˚C and cooled to 0˚C. In the second cycle, these films were again heated to 200˚C and cooled to the 0˚C. Figure 28, shown below, displays a typical DSC scan for a heating and cooling cycle for PVF_2. The heating cycle clearly shows the melting endotherm with T_m (peak) at 162˚C. In the cooling cycle, the crystallization exotherm begins at 137˚C. The area under the melting endotherm and the crystallization exotherm, T_c, represent the enthalpy of melting, ΔH_m, and the enthalpy of crystallization, ΔH_c, respectively. This information can be used to estimate the percent crystallinity and to evaluate the relative crystallinity of the PVF_2 in composites of different composition and thermal history.

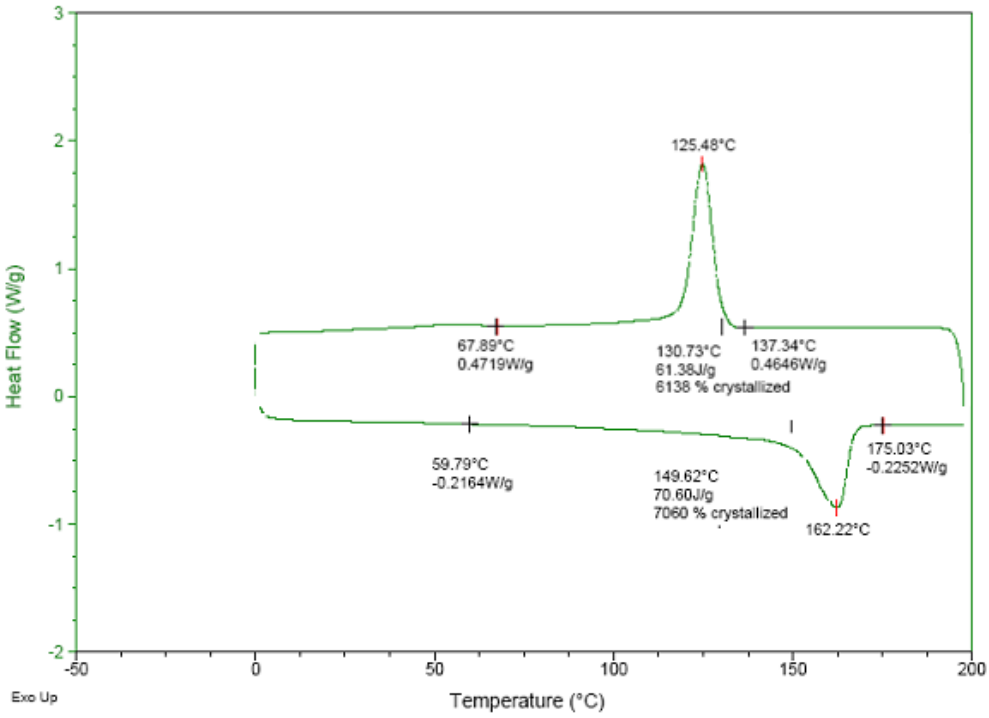

Figure 28. Heating and cooling cycle scans in DSC of Kynar®301 PVF_2

The crystallinity of a semi-crystalline polymer sample can be calculated based on the ratio of enthalpy of melting to the melt enthalpy of a 100% crystalline material. In the present research, the percent crystallinity (%) was simplistically determined using the relationship

$$\% \text{ Crystallinity} = \Delta H_m/\Delta H_m^\circ \times 100\%$$ [39]

Where ΔH_m is the measured enthalpy of fusion, and ΔH_m° is the enthalpy of fusion of a 100% crystalline material. The theoretical latent heat of fusion for 100% crystalline PVF_2, ΔH_m°, was taken to be 104.6 J/g[40]. The composite films of PVF_2 and PVIm/Im^+TFSI^- were cast from DMF and DMAC at ambient temperature and dried at 100˚C. In the DSC, the films were heated to 200˚C and then cooled to 0˚C at 10-20˚C per minute. The heat of melting, ΔH_m, and crystallization, ΔH_c, were determined by integrating the areas (J/g) under the peaks. Films of pure PVF_2 and the PVF_2//PVIm/Im^+TFSI^- composites, were cast from DMAC and DMF. Their thermal properties were examined using DSC and their thermal signatures were studied according to the protocol previously described (See Section I-1, page 22). Each sample was examined by DSC in two 20˚C/min heating and cooling cycles. The X-ray diffraction analysis (see Section III-B-1) already determined that in the first cycle, the PVF_2 in the films cast at ambient temperature and dried below 100˚C, is β-phase. However, PVF_2 recrystallizes to α-phase

after heating to 200˚C. Accordingly, after the first heating cycle, the structure of PVF_2 in the films changed to α-phase. Depending on the crystalline structure before or after the heating cycles are performed, the crystallinity of each sample may be calculated differently. If the phase structure changes during the cycle, crystallinity can only be reasonably determined by the relation given above. If the phase structure does not change, the crystallinity may be determined by $\Delta H_m/H_m^\circ$ or $X_c = (\Delta H_a - \Delta H) / (\Delta H_a - \Delta H_c)$[41], where ΔH_a is the heat capacity associated with the amorphous material. In the present work, percent crystallinity for pure PVF_2 was evaluated by using the simple relationship $\Delta H_m / \Delta H_m^\circ$ instead of the more commonly used relationship $X_c = (\Delta H_a - \Delta H) / (\Delta H_a - \Delta H_c)$. This tactic was chosen because in the first heating cycle, the melting endotherm is for melting of β-phase crystals and the recrystallization exotherm is for the formation of α-phase crystals. The more complex relationship could have been used for the second heating cycle in which α-phase crystals were melting and α-phase crystals were formed on cooling. However, for comparative consistency, the simple $\Delta H_m/\Delta H_m^\circ$ relationship was used.

b. Analysis of DSC thermgrams of PVF_2 and PVF_2//PVIm/Im^+ composites cast from DMAC

The first heating scan of pure PVF_2 cast from DMAC and dried at temperatures below 100˚C is displayed in the Figure 29a. The pure PVF_2 has a melting temperature, T_m, of about 170˚C. The area under the melting endotherm represents an enthalpy of fusion, ΔH_f, which is about 37.5 J/g, and the degree of crystallinity is determined to be 35.8%.

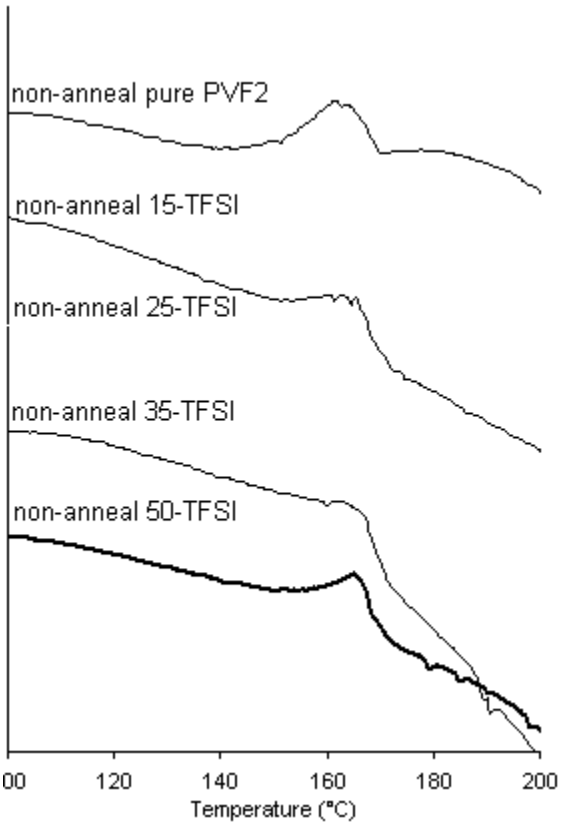

Figure 29a DSC thermograms for the 1st heating scan of non-heated film of PVF_2 and the composites from DMAC

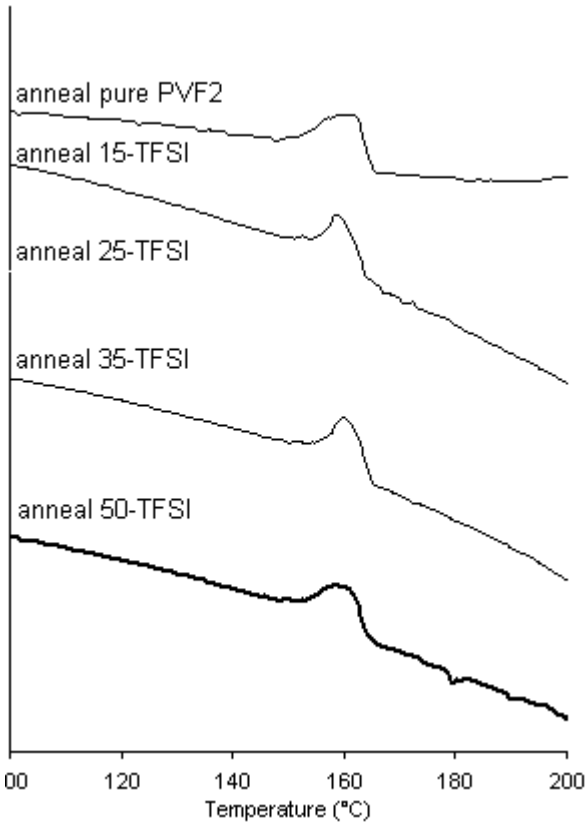

Figure 29b DSC thermograms for the 2nd heating scan of non-heated film of PVF_2 and the composites from DMAC

The first heating scan of the composite films cast from DMAC shows that the melting temperature, T_m, for the initially formed β-phase of PVF_2 is 170-174˚C, similar to T_m (170˚C) of the initially formed β-phase of PVF_2 in homopolymer films. The apparent enthalpy of fusion, ΔH_f, of the initial β-phase of PVF_2 in the composite film is lower than that of pure PVF_2; however, since the composites are only 80 wt% PVF_2 the % crystallinity is actually larger than for pure PVF_2. The value of ΔH_f of the composites in which PVIm was protonated with 25, 35 and 50 mol% TFSI are close (27-33 J/g). This corresponds to a % crystallinity of 36-40% based on PVF_2. The numeric data for the first heating cycle is shown in Table 1a.

Table 1a. DSC results for first hearing scans for homopolymer PVF_2 and composite films of PVF_2 (Kynar®301F) and PVIm/Im^+TFSI^- cast from DMAC

First Heating Cycle			
	T_m (˚C)	Δ H_f (J/g)	% Crystallinity
non- heated pure PVF_2 DMAC	170.20	37.53	35.81%
non- heated 15-TFSI DMAC	171.80	33.53	39.99%
non- heated 25-TFSI DMAC	172.00	28.46	33.95%
non- heated 35-TFSI DMAC	174.03	26.85	32.03%
non- heated 50-TFSI DMAC	170.15	29.00	34.59%

In the second heating cycle, the character and level of α-phase PVF_2 crystals are probed. For pure PVF_2 films cast from DMAC, the T_m of α-phase PVF_2 is about 165˚C; the ΔH_f is 24.65 J/g; and the percent crystallinity is 23.52%. The T_m of α-phase PVF_2 in the composites is between 164 and 166˚C and is similar to that in the homopolymer. When taken on a PVF_2 basis, the ΔH_f of α-phase PVF_2 in the composite films protonated with 15, 25 and 50 mol% TFSI is greater than that of α-phase PVF_2 in the homopolymer. That for the 35 mol% TFSI composite is comparable to that of pure PVF_2 (See Table 1b)

Table 1b. DSC results for second hearing scans for homopolymer PVF_2 and composite films of PVF_2 (Kynar®301F) and PVIm/Im^+TFSI^- cast from DMAC

Second Heating Cycle			
	T_m (˚C)	Δ H_f (J/g)	% Crystallinity
heated pure PVF_2 DMAC	165.38	24.65	23.52%
heated 15-TFSI DMAC	164.77	23.46	28.04%
heated 25-TFSI DMAC	165.86	21.08	25.19%
heated 35-TFSI DMAC	166.60	18.52	22.13%
heated 50-TFSI DMAC	164.72	22.33	26.68%

c. *Analysis of DSC thermograms of PVF_2 and PVF_2//PVIm/Im^+ composites cast from DMF*

The first heating scan of pure PVF_2 cast from DMF and dried below 100˚C is displayed in Figure 30a. The pure PVF_2 has a peak melting temperature, T_m, of about 171˚C. The area under the melting endotherm represents an enthalpy of fusion, ΔH_f, which is about 37 J/g, and the degree of crystallinity is determined to be 35%. The T_m, ΔH_f and percent crystallinity values tabulated for homopolymer films cast from DMF are similar to those in films cast from DMAC. (See Table 1a-line 1 and Table 2a-line 1).

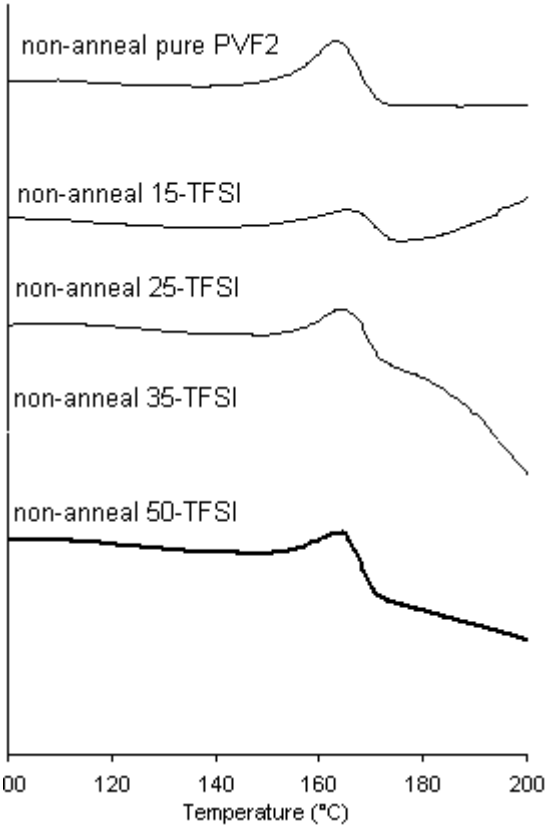

Figure 30a DSC thermograms for the 1st heating scan of non-heated film of PVF_2 and the composites from DMF

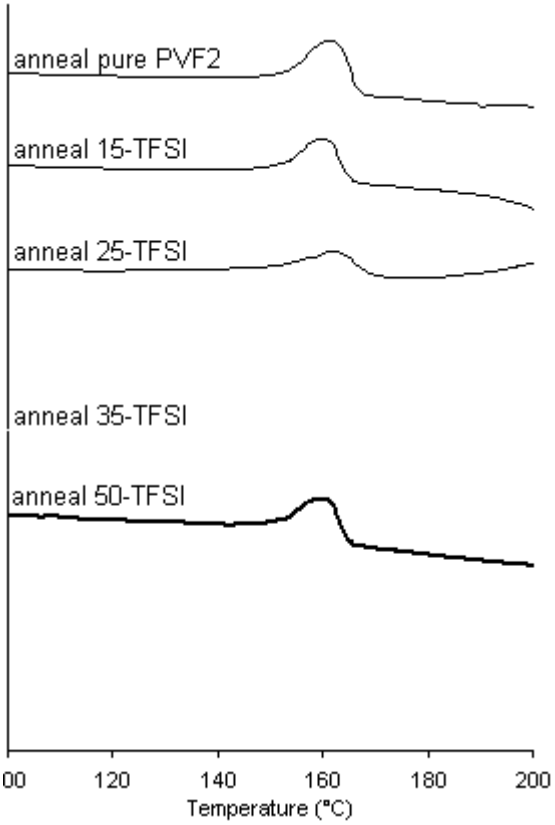

Figure 30b DSC thermograms for the 2nd heating scan of non-heated film of PVF_2 and the composites from DMF

The first heating scan of the composite films cast from DMF shows that the peak melting temperature, T_m, for the initial β-phase of PVF_2 is comparable to that of the β-phase PVF_2 in homopolymer films. Except for the 15 mol% TFSI sample, the enthalpy of fusion, ΔH_f, of the initial β-phase PVF_2 in the composite film is comparable to that of homopolymer film when taken on a PVF_2 basis. The crystallinity of the composites protonated with 15 mol% TFSI was significantly lower than that in pure PVF_2. Given the upward curvature of the trace for the 15

mol% TFSI sample, the integrated area under the peak was difficult to measure. As a result, the measured ΔH_f, of the initial β-phase PVF_2 in the 15 mol% composite film might be low. The crystallinity and ΔH_f of the composites protonated with 50 mol% TFSI is higher than that in composites protonated with 15, 25 and 35 mol% TFSI. The numeric data for the first heating cycle is shown in Table 2a.

Table 2a. DSC results for first hearing scans for homopolymer PVF_2 and composite films of PVF_2 (Kynar®301F) and PVIm/Im^+TFSI^- cast from DMF

First Heating Cycle			
	T_m (˚C)	**ΔH_f (J/g)**	**% Crystallinity**
non-heated pure PVF_2 DMF	**171.14**	**36.98**	**35.29%**
non- heated 15-TFSI DMF	**174.11**	**18.61**	**22.24%**
non- heated 25-TFSI DMF	**171.59**	**28.99**	**34.64%**
non- heated 35-TFSI DMF	**171.84**	**28.68**	**34.27%**
non- heated 50-TFSI DMF	**170.82**	**32.35**	**38.66%**

Given that the literature reports that the T_m of α-phase PVF_2 to be 166-167˚C[42], the T_m measured in the second heating scan for pure PVF_2 cast from DMF is consistent with it being α-phase. Table 2b shows that, in the second heating cycle, pure PVF_2 cast from DMF exhibits a melting temperature, T_m, of about 167˚C, enthalpy of fusion, ΔH_f, about 25.5 J/g, and the degree of crystallinity of about 24%. The T_m of α-phase PVF_2 in composites is 165-169˚C, similar to that in the homopolymer. The ΔH_f of α-phase PVF_2 in the composite films protonated with 25, 35 and 50 mol% TFSI is close (within 1-5 J/g) to that of α-phase PVF_2 in the homopolymer. That for the 15 mol% TFSI composite is about 25% lower when taken on a PVF_2 basis. The numeric data for the second heating cycle is shown in Table 2b.

Table 2b. DSC results for second hearing scans for homopolymer PVF_2 and composite films of PVF_2 (Kynar®301F) and PVIm/Im^+TFSI^- cast from DMF

	Second Heating Cycle		
	T_m (˚C)	Δ H_f (J/g)	% Crystallinity
heated pure PVF_2 DMF	166.72	25.55	24.38%
heated 15-TFSI DMF	168.72	15.11	18.06%
heated 25-TFSI DMF	164.91	20.55	24.56%
heated 35-TFSI DMF	167.39	20.86	24.93%
heated 50-TFSI DMF	165.06	23.87	28.53%

Films rapidly cooled from the melt exhibit lower crystallinity than films cast from solution with no thermal history. This may simply be the result of the trade off between the rate of cooling and the rate of crystallization.

d. Comparative analysis of crystallinity and T_m of PVF_2 and PVF_2//PVIm/Im^+ films cast from DMAC and DMF

The relative crystallinity of PVF_2 homopolymer films and PVF_2//PVIm/Im^+ composite films cast from DMF and DMAC in their first and second heating cycles is tabulated in Table1 and 2 and is graphically displayed in Figures 31 and 32.

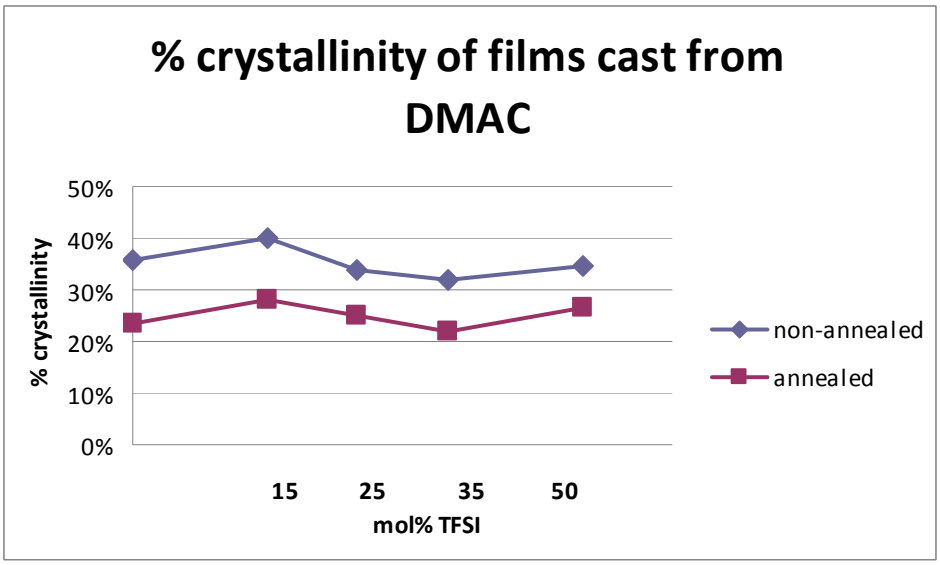

Figure 31. Non-heated and heated films of PVF_2 and composities cast from DMAC.

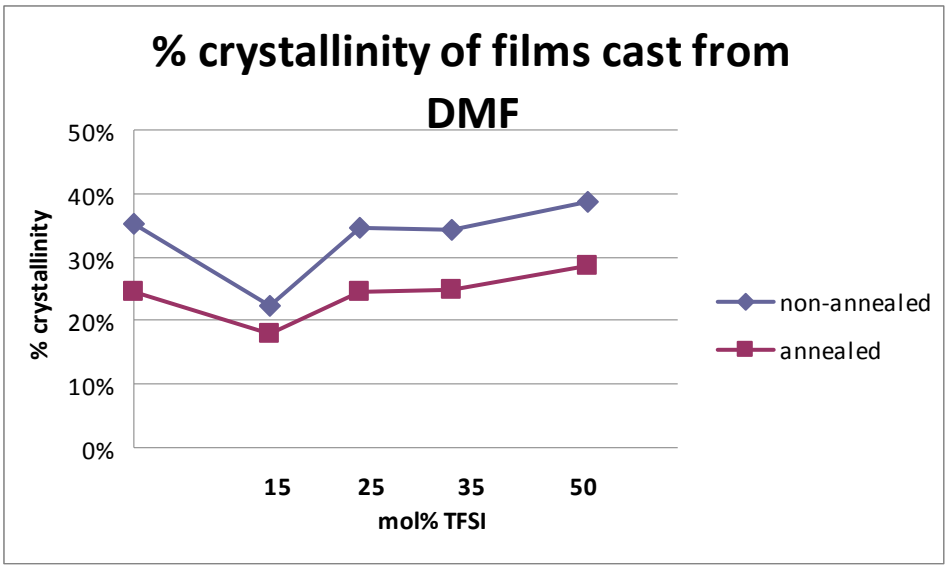

Figure 32. Non-heated and heated films of PVF_2 and composities cast from DMF

T_m values tabulated in Table1 and 2 are graphically displayed in Figure 33. Figure 33 shows the T_m for pure PVF_2 and the T_m for 15, 25, 35 and 50 mol% of TFSI compositions of the PVF_2/PVIm-Im^+TFSI^- system cast from DMAC and DMF.

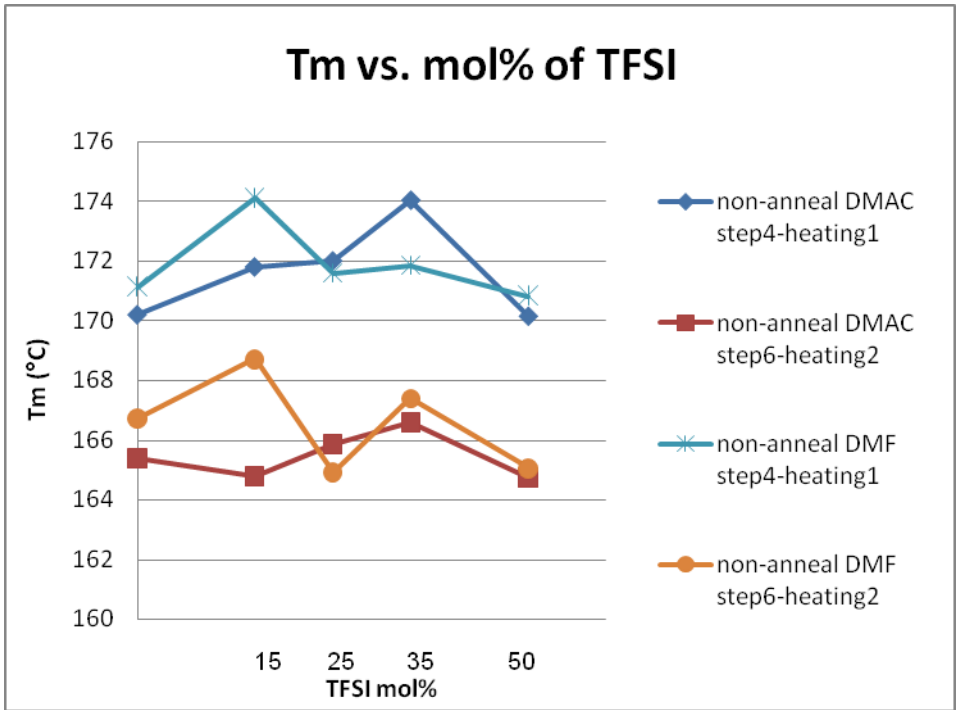

Figure 33. Melting temperture of PVF_2/poly[4(5)-VIm/VIm^+TFSI^-] $(4/1)_v$ in DMF and DMAC

In the Figure 33, one can see that, in the first heating cycle, thermograms of films cast from both DMF and DMAC exhibit a melting peak at 170-174˚C. The melting temperatures of these films in the second heating cycle, i,e., after being heated to 200˚C and rapidly cooled to -70˚C, are lower than those of the non-heated films. It appears that the crystalline phases in non-heated and heated films are different. The X-ray data described in Section III-B-1 teaches that, as cast from DMF and DMAC homopolymer and composite films contain β-phases PVF_2 crystals and that films heated to 200˚C contain α-phase PVF_2 crystals. The T_m of β-phase crystals in pure PVF_2 (first heating cycle) is higher than that of α-phases crystals in the pure PVF_2 (second heating cycle). In the composite films with PVIm/Im^+, the T_m of β-phase crystals of PVF_2 is similarly greater than that of α-phase crystals. The literature[42] reports that the T_m of β-phase PVF_2 is about 172˚C and that the T_m of α-phase PVF_2 is 166-167˚C. In the present work, the T_m of pure β-phase PVF_2 in the homopolymer cast from DMF was measured to be 171˚C and that for films cast from DMAC was 170˚C. These T_m values are consistent with the literature values for β and α-phases.

e. Discussion and analysis of latent heat of crystallization

T_c is the temperature at which recrystallization starts. T_c is always less than the T_m.and the difference is representative of the degree of super cooling required to induce crystallization. No matter if PVF_2 is in the first or second cooling cycle, once it has been heated to 200°C, PVF_2 will recrystallize as α-phase. Figures 34a and 34b show stack plots of the crystallization exotherms observed on cooling films of PVF_2 and PVF_2//PVIm/Im^+ that had been heated to 200°C. It is clear from these cooling curves that there is a significant difference in the recrystallization behavior of films cast from DMF and films cast from DMAC.

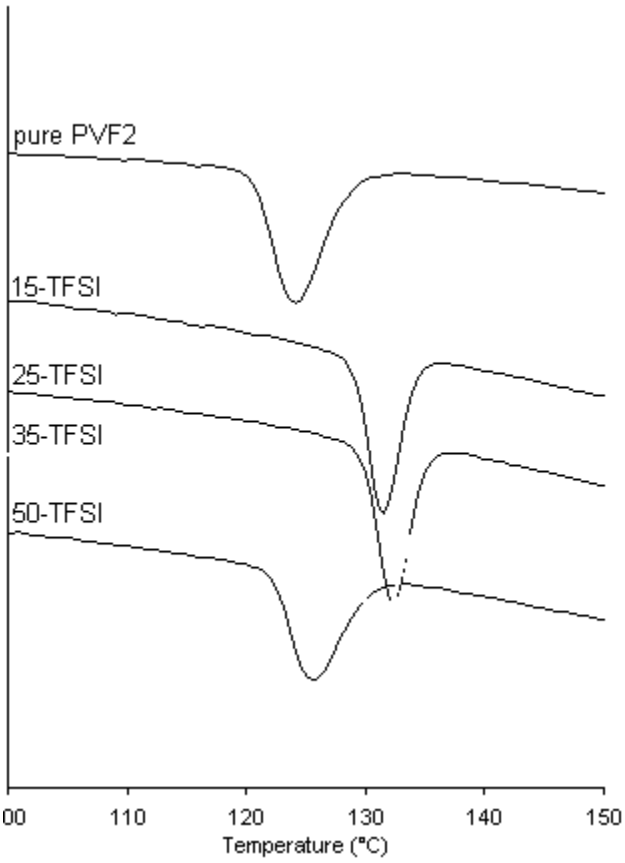

Figure 34a DSC thermograms for the cooling scan of non-heated film of PVF_2 and the composites from DMAC

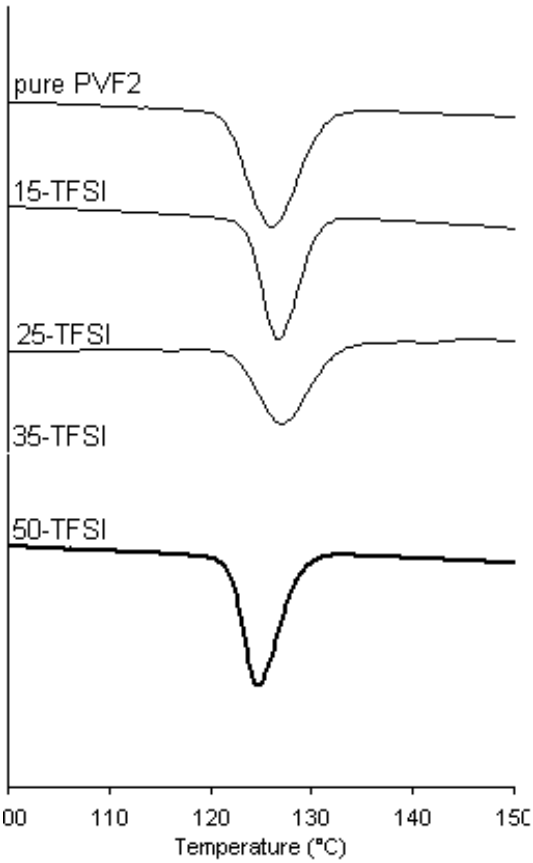

Figure 34b DSC thermograms for the cooling scan of non-heated film of PVF_2 and the composites from DMF

Table 3 tabulates the peak crystallization temperature, T_c, for PVF_2 homopolymer films and composite films of PVF_2//PVIm/Im^+TFSI^-.

Table 3. DSC results for the cooling scan for composite films cast from DMAC and DMF

	Material and Thermal History	Onset T_c (˚C)
Cooling Cycle (DMAC)	non- heated pure PVF_2 DMAC	124.15
	non- heated 15-TFSI DMAC	131.60
	non- heated 25-TFSI DMAC	132.27
	non- heated 35-TFSI DMAC	131.26
	non- heated 50-TFSI DMAC	125.52
Cooling Cycle (DMF)	heated pure PVF_2 DMF	126.16
	heated 15-TFSI DMF	127.17
	heated 25-TFSI DMF	126.84
	heated 35-TFSI DMF	125.15
	heated 50-TFSI DMF	124.82

If the onset T_c data in Table 3 is plotted as a function of the composition of the films and the solvent from which the film was cast, this difference becomes more apparent. Figure 35 shows that the onset T_c of pure PVF_2 in a film, cast from DMAC, is about 129˚C, and that the onset T_c of pure PVF_2 in a film cast from DMF is about 131˚C. Moreover, the onset T_c of each of these films in the first and second cycles, without regard to whether it was cast from DMAC or DMF, is nearly identical. This is a result of the fact that the crystal habit of the PVF_2 recrystallizing in cycle one and cycle two is α-phase. The T_m of α-phase PVF_2 crystals in the homopolymers cast from DMAC and DMF is 166-167˚C (see **Tables 1b and 2b**). The difference between T_m and T_c is the degree of supercooling required to cause recrystallization. Thus, the data shows the degree of supercooling required to recrystallize pure PVF_2 in films cast from DMAC is 38˚C and that degree of supercooling required to recrystallize pure PVF_2 in films cast from DMF is 35˚C. The degree of supercooling required to recrystallize PVF_2 in films cast from DMAC is thus 3° greater than that required to recrystallize PVF_2 in films cast from DMF.

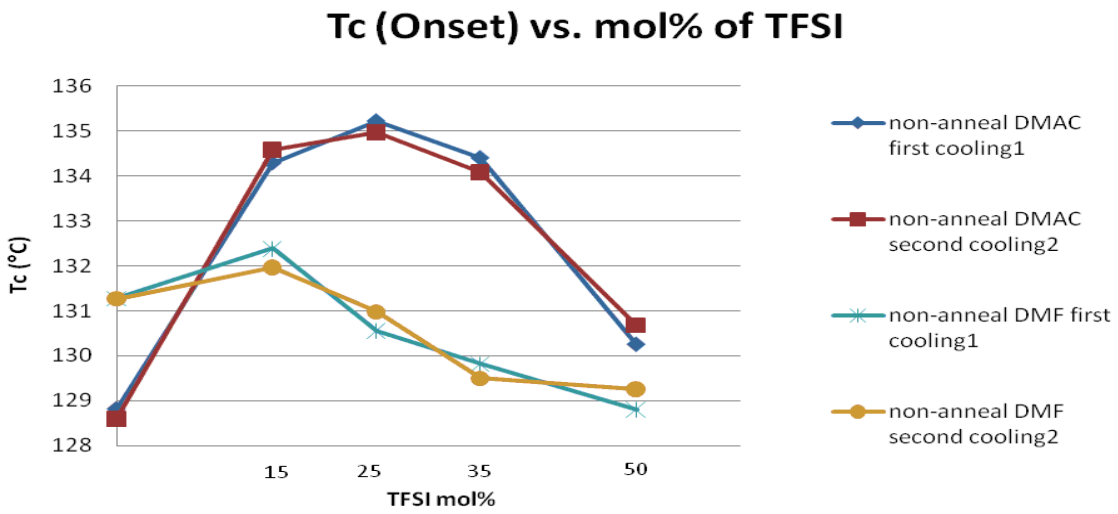

Figure 35. Onset T_c of PVF_2/poly[4(5)-VIm/VIm^+TFSI^-] (4/1)v in DMF and DMAC

The onset T_c of each composite film cast from DMAC or DMF in the first and second cycles are also similar. In composites, the T_c of the films cast from DMAC ranges from 130-134˚C, while the T_c of the composite films cast from DMF ranges from 129-132˚C. The T_m of α-phase PVF_2 crystals in the composites cast from DMAC and DMF is 165-168˚C (see **Tables 1b and 2b**), accordingly, the degree of supercooling required to recrystallize PVF_2 in composite films cast from DMAC is less than that required to recrystallize PVF_2 in composite films cast from DMF.

Recrystallization is invariably a nucleated process. Thus, it appears that the nucleation rate in films of pure PVF_2 cast from DMF is greater than the nucleation rate in films of PVF_2 cast from DMAC. However, when blended with PVIm/Im^+TSFI^-, the nucleation rate in films cast from DMF is less than that in composite films cast from DMAC. The difference between the T_c of the PVF_2 homopolymer films cast from DMAC and DMF is about 5˚C while the difference between T_c of PVF_2 crystals in the composite cast from DMF with 15 mol% TFSI and the T_c of the PVF_2 homopolymer cast from DMF is only about 1˚C.

The difference between the T_c of PVF_2 in a homopolymer film cast from DMAC and a composite cast from DMAC with 15 mol% TFSI is 5-6°C. The big difference in T_c here is indicative of an increased nucleation rate in the composite films cast from DMAC. Figure 35 also shows a trend of decreasing T_c with increasing mol% TFSI. The T_c of PVF_2 in films cast from DMAC starts to decrease when the level of TFSI is 35 mol% or greater. The T_c of PVF_2 in composite films cast from DMF starts to decrease when the level of TFSI is greater than 15 mol%. This suggests that PVIm/Im^+ becomes more compatible at high TFSI levels and the nucleation rate drops. This also indicates that PVIm/Im^+ is less well solvated by DMAC then by DMF.

3) Extractability

Because PEMs must work in an aqueous environment and because protonated PVIm is soluble in water, extraction of PVIm by aqueous solutions and determination of the associated weight loss is an important test. If the PVIm/Im^+ phase is intimately mixed with the amorphous phase of PVF_2 or if it is covalently linked to the PVF_2 amorphous phase, it will not be easily extracted from the composite. On the other hand, if phase separation is macroscopic, the PVIm/Im^+ might be substantially extracted from the composite.

Accordingly, water extraction studies give us practical information about the utility of a composite membrane in the aqueous environment of a working fuel cell membrane electrode assembly or fuel cell stack. Moreover, water extraction studies can give one inferential information relating to the intimacy of the distribution of the PVIm/Im^+ component.

Wu's PVF_2//PVIm/Im^+TFSI^- composite films were extracted with distilled water for 48 hours at ambient temperature, dried to constant weight, and heated for 5 minutes at 200˚C. The

8/1, 4/1 and 3/1 films lost 16.7, 26.1 and 30% of their original mass, respectively. When the films were doped with 0.1 mole% of dibenzoyl peroxide prior to heating at 200˚C for 5 minutes, the 8/1, 4/1 and 3/1 films lost 2.6, 3.1 and 7.6% of their original mass, respectively. The differential was due to crosslinking of the films doped with BPO prior to heating to 200˚C.

In the present work, water extraction of Kynar®301 PVF_2/poly[(4(5)-VIm/VIm^+TFSI^-] composite films was carried out in accordance with the protocol described in the experimental section, II-H-4. The heated composite films with 15, 25, 35 and 50 mol% of TFSI lost no mass. The non-heated composite films with 15, 25, 35 and 50 mol% of TFSI lost only 4.13, 1.93, 0.34 and 1.62% of their original mass, respectively. PVIm is more soluble in ethanol/water than in water. Accordingly, extraction experiments were repeated with the present set of materials, extracting with ethanol/H_2O $(1/1)_v$.

Water/ethanol extraction of Kynar®301 PVF_2/poly[(4(5)-VIm/VIm^+TFSI^-] composite films was carried out in accordance with the procedure described in section II-I-4. The heated composite films with 15, 25, 35 and 50 mol% of TFSI lost 16.20, 11.36, 6.56 and 15.16% of the mass associated with PVIm/Im^+, respectively. The non-heated composite films with 15, 25, 35 and 50 mol% of TFSI lost 81.00, 72.72, 75.44 and 68.84% the mass associated with PVIm/Im^+, respectively. The data is summarized in Table 4.

Table 4. Percent of PVIm/Im^+TFSI^- Extraction with Ethanol/H_2O $(1/1)_v$

	15 mol%TFSI	**25 mol%TFSI**	**35 mol%TFSI**	**50 mol%TFSI**
Heated films	16.20%	11.36%	6.56%	15.16%
Non- heated films	81.00%	72.72%	75.44%	68.84%

Surprisingly, the percent extracted from the present set of composites as a function of percent TFSI was much lower than was observed by Wu. In these experiments, (vinylidene fluoride/hexafluoropropylene) (Kynar® 2801) and (vinylidene fluoride/tetrafluoroethylene) (Kynar® 7201) composites were also examined. It was expected that the fraction of amorphous fluoropolymer phase would be higher in the copolymer and that the mixing of the PVIm/Im^+TFSI^- with the amorphous phase might be enhanced in PVF_2 copolymer composites. The results without BPO in the present work are graphically displayed in Figure 36. In the figure, 301 annealed, 2801 annealed, and 7201 annealed identify Kynar® 301 PVF_2//PVIm/Im^+TFSI^-, Kynar® 2801 PVF_2//PVIm/Im^+TFSI^- and Kynar® 7201 PVF_2//PVIm/Im^+TFSI^- composites.

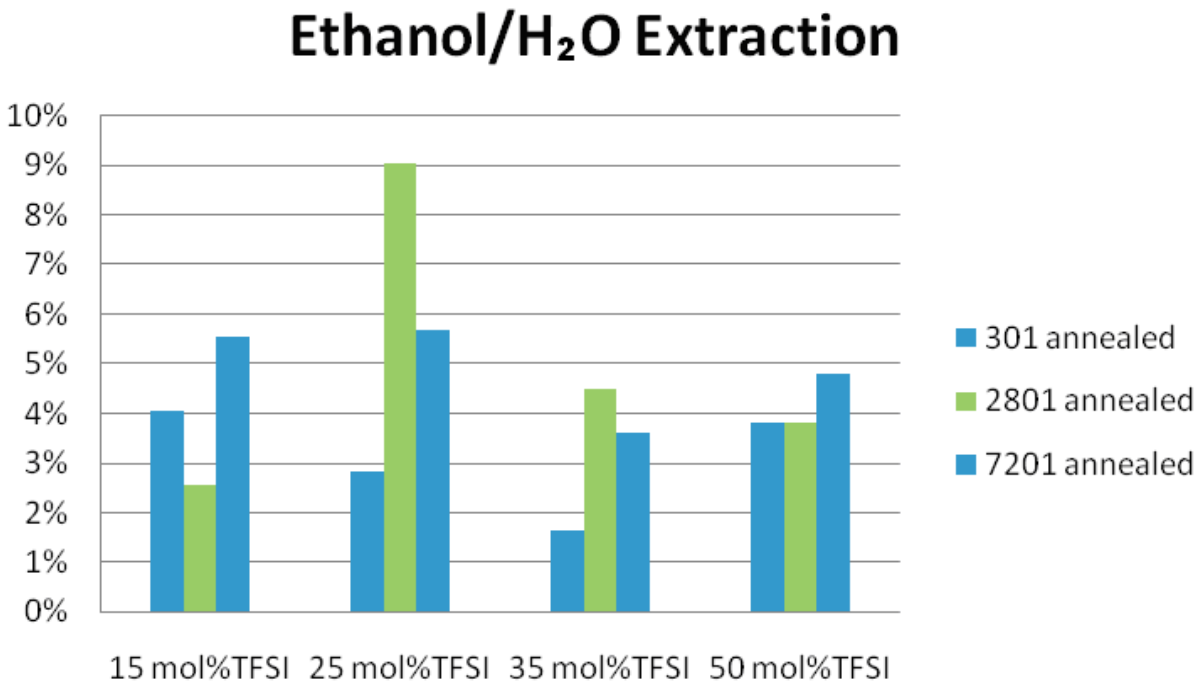

Figure 36. Comparison ethanol/water extractions in different composites

One can see that the percent extractables of all heated composites was less than 10%. PVF_2 composites were generally less extractable than the PVF_2 copolymer composites, with extractable $PVIm/Im^+$ always being less than 5%. If the $PVIm/Im^+$ had been fully extracted, that percent extractables would have been 20%. At the present time, the difference between the extraction results obtained by Wu and the results obtained in the present research cannot be rationalized. Originally, it was thought that there might be some difference in the molecular weight of PVIm used by Wu (polymerized with AIBN in benzene) and PVIm used in the present experiments [polymerized with 4,4-azo-*bis*(4-cyanovaleric acid) in ethanol/H_2O]. Indeed, viscometric studies show that PVIm polymerized in ethanol/H_2O is lower in molecular weight than that obtained from benzene. Does this mean that the lower molecular weight $PVIm/Im^+$ is more miscible in PVF_2 than and therefore contributes more to reduction in extractability then does higher molecular weight?

IV. Summary

Wu conducted hot-stage microscopic studies to show that PVF_2 crystallite size is sub-microscopic, in films heated to 200˚C. Larger micron-sized spherulites were observed in films cast from DMF and dried at temperatures below 100˚C. The crystal habit of the PVF_2 in the heated and non-heated films was not determined. In addition, in Wu's work, only one level of TFSI (50 mol%) was evaluated.

The main advance in the present work is the evaluation of the crystal habit of PVF_2//PVIm/Im^+TFSI^- composites by X-ray diffraction. The mol% TFSI was varied from 15 mol% to 50 mol%. The lower level was chosen to span optimum level of TFSI in Watanabe's studies of monomeric imidazole/imidazolium TFSI mixtures.[33] By analysis of X-ray diffraction data, it was determined that PVF_2 in "non-heated films", i.e. films that were dried at temperatures below 100°C, predominantly adopted the crystalline β-phase, and PVF_2 in "heated films", i.e., films that had been heated to 200°C, predominantly adopted the crystalline α-phase. The habit of PVF_2 crystals in the composite films was found to be the same as that in pure PVF_2 films. The percent crystallinity determines the volume fraction of the amorphous PVF_2 phase which is mixed, at some microscopic or sub-microscopic scale, with PVIm/Im^+TFSI^-. The presence of PVIm and the percent protonation with TFSI appears to influence the nucleation process of the PVF_2 crystalline domains; acting as a nucleating agent. Restriction of the PVIm/Im^+ to thread-like structures permeating the amorphous phase would account for the substantial conductivity observed by Wu. The implications of this research allows us to construct the following microscopic picture of an initially-formed composite having β-phase crystals that, when heated to 200°C and rapidly cooled, recrystallize to yield a more intimate composition in which the crystalline polymorph is α-phase. In DSC studies, the higher T_m of PVF_2 in the initially formed poly[4(5)-VIm/VIm^+TFSI^-] composite films is consistent with the X-ray diffraction assignment as β phase of PVF_2. Similarly, the lower T_m of PVF_2 in the poly[4(5)-VIm/VIm^+TFSI^-] composite films that had been heated to 200°C is consistent with the X-ray assignment as α-phase of PVF_2. Based on the X-ray diffraction data, DSC analysis, crystallinity and extractability, the microstructure and morphology of PVF_2/poly[4(5)-VIm/VIm^+TFSI^-] composite films can be envisioned. The PVF_2 amorphous phase is the major component, ~40%.

The PVF_2 crystals (20-35%) are uniformly distributed in the amorphous PVF_2 continuum. The $PVIm/Im^+$ (~20%) is also distributed in the amorphous PVF_2 phase.

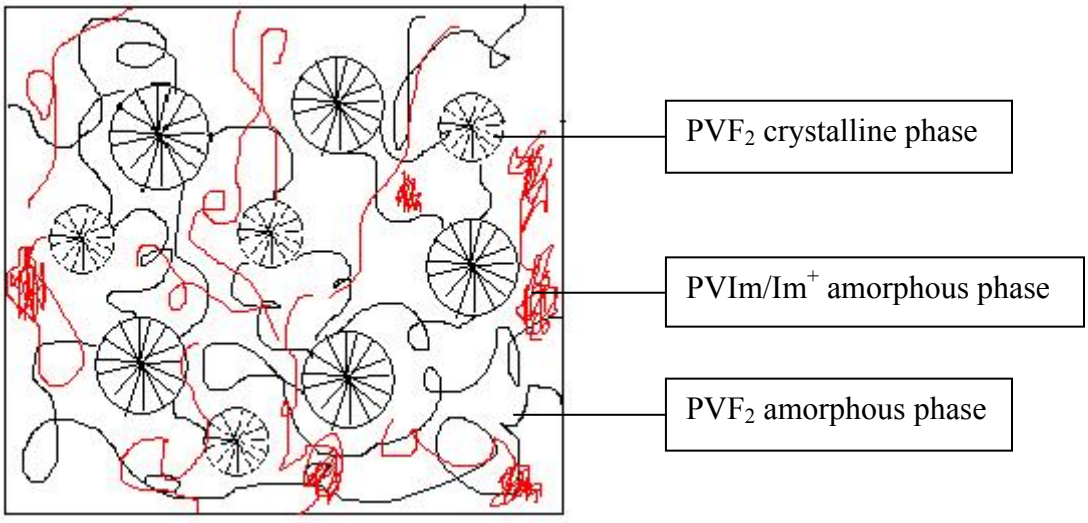

Figure 37. Visualized microstructure of PVF_2/poly[4(5)-VIm/VIm^+TFSI^-] composites

Figure 37 shows a cartoon reflecting a submicroscipic picture of a PVF_2//poly[4(5)-VIm/VIm^+TFSI^-] composite. In the cartoon, three phases are depicted: 1) PVF_2 crystallites/spherulites, 2) PVF_2 amorphous chain segments and 3) amorphous $PVIm/Im^+$ polymer. The black radial structures represent crystalline spherulites of PVF_2 tethered by amorphous PVF_2 chain segments, also colored black. $PVIm/Im^+$ is shown as red squiggles and is dispersed within the amorphous PVF_2 phase. The scale at which it is separated from the PVF_2 amorphous phase is not known, however, based on the relative clarity (transparency) of the heated films, the dimensions of the PVIm/Im+ phase must be less than the wavelength of visible light. The increase clarity of composites containing 35 and 50 mol% TSFI indicates that the miscibility of $PVIm/Im^+$ with the amorphous phase of PVF_2 increases at higher TFSI levels. It is yet to be determined what TFSI level is optimum for high proton conductivity, mechanical strength and chemically stability.

V. **References**

1 "Global Warming", The New York Times, **2009**. http://topics.nytimes.com/topics/news/science/topics/globalwarming/# (accessed May 2009).

2 Snyder, R. E. "Oil supply limitations drive price increases" http://findarticles.com/p/articles/mi_m3159/is_5_225/ai_n27796744 (accessed May 2009).

3. Grove, William Robert "On a Gaseous Voltaic Battery", *Philosophical Magazine and Journal of Science* **1842** *vol. XXI*, pp 417-420.

4 U. S. Department of Energy, "How they work: PEM Fuel Cells" – www.fueleconomy.gov. (accessed May 2009)

5 The Online Fuel Cell Information Resource, http://www.fuelcells.org/basics/types.html (accessed May 2009).

6 Curtin, S. Different Types of Fuel Cells, *The Alternative Energy Emagazine*, 2006. http://www.earthtoys.com/emagazine.php?issue_number=06.04.01&article=fuelcells. (accessed May 2009).

7. Grot, W. *Chem. Ing. Tech.,* **1978**, *50(4)*, 299-301.

8 Ren, X.; Wilson, M.S.; Gottesfeld, S. *J. Electrochem. Soc*, **1996,** *L12*,143.

9 Schmidt-Rohr, K., Figure 2 in *"Water Nanochannels in Nafion®: Quantitative Scattering Analysis by NMR,"* DOE Progress Report, Program Officer Richard Kelly. http://www.hydrogen.energy.gov/pdfs/review07/bes_5_schmidt-rohr.pdf (accessed May 2009).

10 Kreuer, K.D. *J. Membr. Sci.,* **2001**, *185*, 29-39.

11 Fuller, A.; Breda, A.C.; Carlin, R.T. *J. Electrochem. Soc.,* **1997**, *144*, L67.

12 Kynar® & Kynar Flex® PVDF Performance Characteristics & Data, Atofina. http://www.arkema-inc.com/kynar/page.cfm?pag=1006 (accessed May 2009).

13 Partridge, R. "Fire-Resistant Foams for Pharmaceutical and Semiconductor Cleanrooms," *Controlled Environments*, **2007**. http://www.arkema-inc.com/kynar/page.cfm?pag=1117 (accessed May 2009).

14 Kynar Flex & Kynar PVDF Wire and Cable Applications, Arkema ADV#06-302 PP5000-8/06. http://www.arkema-inc.com/kynar/literature/pdf/670.pdf (accessed May 2009).

15 Dennis, G. "Polymer Piping Performance for Pharma and Biotech Applications," **2003**. http://www.arkema-inc.com/kynar/page.cfm?pag=1009 (accessed May 2009).

16 Kynar® PVDF Resin for Battery Manufacture. Arkema. http://www.arkema-inc.com/kynar/page.cfm?pag=1003 (accessed May 2009).

17 Kepler, R.G. Ferroelectric Pyroelectric, and Piezoelectric Properties of Poly(vinylidene Fluoride. In *Ferroelectric polymers: chemistry, physics, and applications*; by Nalwa, H. S.; CRC Press, 1995.

18 Zhang, Q. M.; Bharti, V.; Kavarnos, G. Poly(Vinylidene Fluoride) (PVDF) and its Copolymers. In *Encyclopedia of Smart Materials, Volumes 1-2*; Schwartz, M., Ed.; John Wiley & Sons: 2002; pp 807-825.

19 Nalwa, H. S. *Ferroelectric Polymers: Chemistry, Physics, and Applications*; CRC Press, 1995; p 66.

20 Kreuer, K.D.; Fuchs, A.; Ise, M.; Spaeth, M.; Maier, J. *Electrochim. Acta*, **1998**, *43,* 1281.

21 Susan, M.A.B.H.; Yoo, M; Nakamoto, H.; Watanabe, M. *Chem. Lett.,* **2003**, *32*, 836.

22 Münch, W.; Kreuer, K. D.; Silvestri, W.; Maier, J.; Seifert, G. *Solid State Ionics,* **2001**, *145*, 437

23. Scharfenberger, G.; Meyer, W. H.; Wegner, G.; Schuster, M.; Kreuer, K.D.; Maier, *J. Freudenberg Forschungsdienste KG; Fuel Cells (Weinheim, Germany)*, **2006**, *6(3-4)*, 237-250.

24 Pu, H.; Meyer, W. H.; Wegner, G. *Macromol. Chem. Phys.,* **2001,** *202,* 1478-1482.

25 Bozkurt, A.; Meyer, W.H. *Solid State Ionics*, **2001**, *138*, 259-265.

26 Zhou, Z.; Liu, R.; Wang, J.; Li, S.; Liu, M.; Brédas, J.L. *J. Phys. Chem.,* **2005,** *127,* 10824-10825.

27 Martinelli, A.; Matic, A.; Jacobsson, P.; Boerjesson, L.; Fernicola, A.; Panero, S.; Scrosati, B.; Ohno, H. *J. Phys. Chem. B*, **2007**, *111(43)*, 12462-12467.

28 Fernicola, A.; Panero, S.; Scrosati, B. *J. Power Sources*, **2008**, *178(2)*, 591-595.

29 Watanabe,M.; Uchida,H.; Seki,Y.; Emori,M.; Stonehart, P. *J. Electrochem. Soc.* **1996**, *143***,** 3847.

30 Jinghang, W. Investigation of Poly[4(5)-vinylimidazole] Composites and Their Potential as Proton Conductive Membranes. M.S. Thesis, Rochester Institute of Technology, Rochester, NY, 2006.

31 Overberger, C.G.; Kawakami, Y. *J. Polym. Sci.: Polym. Chem. Ed.,* **1978**, *16,* 1237-1248.

32 http://www.cannoninstrument.com/P10-0126%20Cannon-Ubbelohde%20Semi-Micro%20types%20instructions.pdf (accessed May 2009).

33 Billmeyer Jr, F.W.; *Textbook of Polymer Science*, **1971**, 84-85.

34 Cebe, P. Private communication, **2008**.

35 Benz, M; Euler, W.B.; Gregory, O.J. *Macromolecules* **2002**, *35*, 2682-2688.

36 Kobayashi, M; Tashiro, K.; Tadokoro, H. *Macromolecules* **1975**, *8*, 158.

37 Omar, A. “Processing, Morphology and Product Parameters of PVDF Filaments for Biomedical Applications,” M.S. Thesis, University of Ghent, Ghent, Belgium, 2008. http://lib.ugent.be/fulltxt/thesis/2719_Abid.pdf. (accessed May 2009).

38 Song, D.; Yang, D.; Feng, Z.; *J. Mater. Sci.*, **1990**, *25*, 57-64.

39 Roohani, M.; Habibi, Y.; Belgacem, N.M.; Ebrahim, G.; Karimi, A.N.; Dufresne, A.; *Eur. Polym. J.* **2008**, *44 (8)*, 2489-2498.

40 Nakagawa, K; Ishida, Y. *J Polym. Sci. Polym. Phys. E,* **1973,** *11*, 2153.

41 Rabek, J.F. *Experimental Methods in Polymer Chemistry*; John Wiley & Sons: New York, 1980; p 570.

42 Buckley, J.; Cebe, P.; Cherdack, D.; Crawford, J.; Ince, B.S.; Jenkins, M.; Pan, J.; Reveley M.; Washington, N.; Wolchover, N. *Polymer*, **2006**, *47*, 2411-2422.